Marquette University
e-Publications@Marquette

Master's Theses (2009 -)

Dissertations, Theses, and Professional Projects

Modeling and Validation of a Fault Mitigation Method in Induction Motor-Drive Systems Using Magnetic Equivalent Circuits

Shaohua Suo
Marquette University

MODELING AND VALIDATION OF A FAULT MITIGATION METHOD IN INDUCTION MOTOR-DRIVE SYSTEMS USING MAGNETIC EQUIVALENT CIRCUITS

By

Shaohua Suo, B.S.

A Thesis submitted to the Faculty of the Graduate School,
Marquette University,
in Partial Fulfillment of the Requirements for
the Degree of Master of Science

Milwaukee, Wisconsin

May 2011

ABSTRACT

MODELING AND VALIDATION OF A FAULT MITIGATION METHOD IN INDUCTION
MOTOR-DRIVE SYSTEMS USING MAGNETIC EQUIVALENT CIRCUITS

Shaohua Suo, B.S.
Marquette University, 2011

In this thesis, a fault mitigation method for delta-connected induction motor-drive systems under a two-phase open-delta faulty operating condition is analyzed and verified. More specifically, this fault mitigation technique can provide a set of almost balanced motor line currents, and significantly reduce torque ripples, even when the machine runs under the aforementioned two-phase open-delta faulty operating condition. This condition is analyzed using a Magnetic Equivalent Circuit (MEC) model. This model is developed for a delta-connected induction motor which is coupled to its drive system, including the fault mitigation controller. That is, the MEC model is linked to its associated PWM inverter to include the electronic switching effects. This global motor-inverter model was simulated in a Matlab-Simulink environment, under both healthy and faulty operating conditions, while the inverter is operated in both the open-loop scalar control and closed-loop vector control modes. The results obtained from the global model are compared in this thesis to the results obtained from the corresponding Time-Stepping Finite Element (TSFE) simulation and experimental motor-drive test data. A comparative analysis of the motor performance obtained from these results, under the two-phase open-delta faulty operating case, is presented in this work. The simulation and experimental data show that the delta-connected MEC model can provide reasonably accurate results. Thus, the validity and applicability of the fault mitigation technique is thereby verified.

ACKNOWLEDGMENT

I wish to express special gratitude to my family and friends for their encouragement and support throughout this work. I would like to delicate this work to my parents, who always supported me especially when I was in my most depressed time.

I would like to express my sincere and deep appreciation to my advisor, Dr. Nabeel A.O.Demerdash, for his never ending support, encouragement, and valuable discussions. I should acknowledge members of the examination committee, Dr. Edwin E. Yaz, and Dr. Susan C. Schneider, for their careful review of this work and valuable feedback, as well as useful suggestions that helped to make this work more complete.

Finally, I wish to express special thanks to my laboratory teammates and friends, Gennadi.Y.Sizov, Peng Zhang and Ahmed Sayed-Ahmed, for their discussions, and suggestions about my research topic. However, more importantly, I would like to thank them for their motivation throughout this work.

Table of Contents

List of Figures

Chapter 1
Introduction

1.1 Background

AC induction machines, especially polyphase induction machines presently are widely used in a large variety of industrial installations and applications. The design of these ac induction machines has been revisited and revised over many years since their discovery and the discovery of the magnetic rotating field phenomena by Nikola Tesla in the 1880's [1], and its application to rotating machinery [1, 2]. In the last century, induction machines have been very well developed and applied to the industrial field by the engineers and researchers. One well-known kind of induction machine is the so-called squirrel-cage (rotor) induction machine, and this kind of rotor structure really enhances the reliability and ruggedness of this type of machine, as well as significantly decreases the cost of its operation and maintenance. Thus, these modern squirrel-cage induction machines possess a ruggedness and relative simplicity of design, which results in reduced manufacturing and maintenance costs [3]. Accordingly, these squirrel-cage induction machines are now widely utilized and are now the most common type of induction machines utilized in industry today.

In addition, due to the development in power semiconductor technology in the last few decades and the associated technology of electronic power processing (changing ac voltage, current, and frequency at will), induction machines are being utilized in those adjustable speed drive (ASD) applications, in which one needs complicated and precise control of speed and torque. Moreover, the continued

breakthroughs in the digital electronics field provided significant help in the ac motor-drive area. For example, modern digital processing units with high speed processing capabilities are able to host and execute real-time complex control algorithms for variable/adjustable speed drives (VSDs/ASDs).

Modern induction machines and their drive control systems possess relatively high degree of reliability nowadays. However, being practical devices with parts and components they are still prone to failures. These failures may happen in the machines themselves, such as bearing faults, stator faults, and rotor faults. Bearing-related faults appear to be the most common type of faults according to the survey given in the Electric Power Research Institute's (EPRI) reports and these bearing faults constitute about 41% of motor faults [4]. Bearing-related faults may be caused by improper maintenance, inadequate engineering design, external contamination, and also the fast switching occurring in pulse width modulated (PWM) ASD-motor-drive system [5]. Stator winding short-circuits are estimated to constitute about 36% of ac motor faults according to the abovementioned survey carried out by EPRI in 1985 [6]. These short-circuit faults include inter-turn short-circuit faults, open-coil faults, phase-to-phase short-circuit faults, or phase-to-ground faults. Rotor broken-bar and end ring faults have been also reported in the above survey carried out by EPRI [7], and were reported to constitute about 9% of motor faults. Broken-bar faults are mainly due to thermal and mechanical stresses especially due to frequent starting operations, aging effects and/or manufacturing defects. The fault detection and condition monitoring techniques for squirrel-cage induction machines is another topic and detailed works on this subject are reported in references such as [8]-[10], among

many other works in the literature.

On the other hand, various types of severe faults may also happen in the power-electronics portion (drive) components of motor-drive systems. The main function of ac motor-drive systems is controlling motor terminal currents and voltages in order to achieve reliable control of torque and speed under stable operating conditions. Such torque and speed may be manually selected by the user, or by an automated system in case of automated industrial processes. Such faults in the power electronic portion of motor-drive system may happen in the rectifier bridge, cables, or in the power fuse connecting the inverter bridge to the rectifier [11]-[13]. These faults could constitute catastrophic failure in such motor-drive systems. Nowadays, the widespread use of ac induction motor-drive systems in critical applications require industry to develop and manufacture more intelligent systems with enhanced reliability and survivability, in order to utilize them under severe environmental and other severe operating conditions, such as for example underground mines, deep oil wells, and deep-sea exploration. Therefore, it is significant to develop rigorous fault mitigation techniques in such ASDs and fault tolerant ASD systems for such types of industrial motor-drive applications. Thus arises the need for development of reasonably accurate modeling and simulation techniques for such ASD motor-drive systems under healthy and faulty operating conditions.

1.2 Literature review

In this section, more detailed review of the literature on faults and associated faulty operating conditions in adjustable-speed drives (ASDs), as well as the associated power electronics is given. In addition, this literature review centers on the fault mitigation methods and fault-tolerant drive systems that have been previously published in the literature.

1.2.1 Power electronics converter faults in AC drives

As mentioned earlier, the main purpose of ac induction motor-drive systems is meeting an output torque and speed requirement through controlling motor terminal currents and voltages, while achieving stable operating conditions. One of the main components of a conventional drive in an ac induction motor-drive system is a standard uncontrolled diode rectifier bridge or a thyristor controlled rectifier bridge. The rectifier bridge converts the electrical ac voltage supplied by the electric utility to a dc voltage, and this dc voltage is usually filtered and smoothed by bulk dc link electrolytic capacitors at the so-called dc bus of the drive portion of the system. Another main component of the drive is a dc-to-ac inverter bridge which inverts the dc bus voltage into an ac voltage with an appropriate selected frequency and voltage magnitude [14]. This inverter bridge consists of three legs, and each leg consists of two IGBTs connected in series across the dc link, see the Figure.1.1 [30]. This power structure is the most common one and it has already been applied in numerous industrial and commercial products.
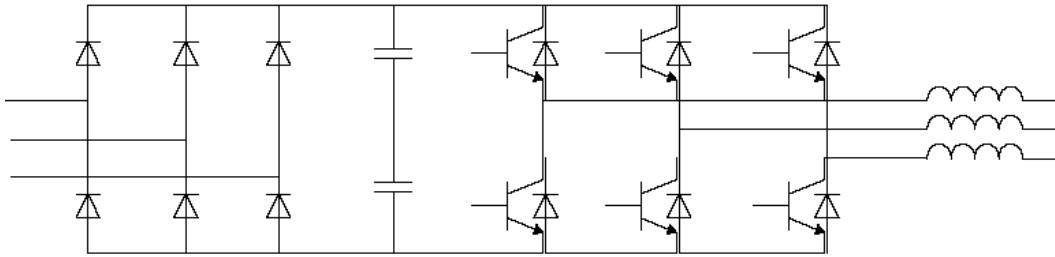
Fig.1.1 A standard power structure for the power converter

Faults may happen in any part of the drive system on the rectifier, filtering capacitor, or inverter bridge. The failures of power switches, IGBTs, constitute the most significant category of failure modes of the drive/power converter. These failures may be caused by external faults, thermal stresses, voltage spikes or other internal failures in the various components of the drive as described in [11]-[13].

As stated in reference [15] "Failure of IGBT power switches in inverter bridges may lead to a single phase motor operation mode. Operating the motor in this faulty mode can cause significant damage to the motor as well as the drive. Single phase operation from the rectifier side can either occurred due to failure in one of the diodes in the rectifier bridge, failure in the cable, or in the power fuses connecting the mains to the rectifier. The single phase motor model operation introduces high voltage and current ripples across the dc link which may cause capacitor failure or undesirable current and torque harmonics [15]". The dc link electrolytic capacitors constitute very critical components in such kind of motor-drive systems and therefore capacitor failure modes and capacitor life prediction have been investigated by researchers, see references [16]-[20].

Typically the dc link electrolytic capacitors have three failure modes, namely, wear-out, early-life and operating-life failures [16]-[20]. Wear-out is the most common failure mode and this kind of failure mode is due to the loss of electrolytic dielectric strength or ESR "equivalent series resistance" increase [19]. Other failure modes may be caused by aging effects, thermal stresses or high current ripples due to either improper design or the existence of other fault condition. Further detailed discussion and analysis on several fault modes in motor-drive systems and power converters can be found in references [21]-[24].

1.2.2 Fault tolerant motor-drive systems

When the faults occur in critical industrial and commercial motor-drive systems, continuous operation of these systems until complete unit failure is very important to avoid catastrophic consequences. These kinds of critical motor-drive systems include water feed pumps in nuclear plants and associated cooling tower functions, ventilation systems in mines, aircraft critical electrical loads and so on. Therefore, numerous designs for fault tolerant motor-drive systems have been proposed, such as for example in [25]-[34].

Early work in the area of fault-tolerant motor-drive systems traces back to 1978 [25] and 1980 [26]. In this work, Jahns introduced the concept of phase redundancy in fault-tolerant motor-drive systems. This technique was based on the fact that an n-phase motor was capable of continued operation with only "n-1" energized phases provided that n>3, and the n-phase drive was capable of withstanding the stresses associated with "n-1" phase operation.

Oliveira proposed in [28] an innovative method to enable balanced operation of three-phase delta-connected induction motors with only one phase (single-phase) supply caused by failure of one of the phases and a small degree of voltage unbalance. This method was based on using a properly designed capacitor in parallel with one of the motor phases in order to minimize or eliminate the backward rotating magneto-motive force (mmf) component in the airgap.

Sepe Jr. proposed in [29] a fault-tolerant motor-drive system in case of current sensors failure or encoder failure in the drive. The basic principle of this method was to provide a smooth transfer from the vector-controlled motor-drive operation to the open-loop constant (V/f) control through proper reconfiguration of the control system that minimized or eliminated transients during the transfer between the two modes.

Sayed-Ahmed introduced to the literature, an advanced fault mitigation method for the delta-connected motor-drive systems, to enable a balanced operation when one phase winding of the machine was disconnected [30]. This technique can produce an almost balanced rotating magneto-motive force (mmf) in the airgap with only two active phase windings. It is based on using appropriate PI controllers on the d-axis and q-axis to eliminate the backward rotating mmf in the airgap, and this technique has no adverse effects on the machine operation under healthy operating condition. This fault mitigation method has been developed and verified by a Time-Stepping Finite Element (TSFE) model coupled to three sinusoidal inputs and a simple Simulink model coupled to a PWM inverter. The detailed principles of this fault mitigation method are explained next in Chapter 2 and the results from the TSFE model will be presented in Chapter 5 of this thesis.

1.2.3 Magnetic equivalent circuit modeling

The Magnetic Equivalent Circuit (MEC) modeling approach has been successfully used to model a variety of electric machines under various healthy and faulty operating conditions. The MEC modeling approach can include the effects associated with the discrete winding distribution, stator and rotor slotting and skewing, as well as the saturation effects which are caused by the nonlinear magnetic material properties [35].

Ostovic proposed in [36] a simplified approach to MEC modeling of an induction machine in 1988. This simplified modeling method is based on neglecting the radial components of rotor and stator slot leakage flux. This model is able to evaluate both time and space variations simultaneously and speed up the computation.

Meshgin-Kelk introduced a three-dimensional MEC model for squirrel cage induction machines and applied this MEC model in the study of inter-bar currents and axial fluxes in healthy and faulty induction machines [37]. Comparison between the simulation results obtained from the MEC model and the experimental results showed that the 3-D MEC model can provide accurate results for both healthy and faulty conditions.

Sizov proposed in [38] a MEC model for induction machines, and applied this model in the study of diagnostics of adjacent and nonadjacent rotor bar breakages for squirrel cage induction machines. The model has been later extended in [39] to include stator faults. This MEC model was implemented in a Matlab-Simulink environment which includes the effects of the discrete winding distribution, rotor and stator slotting and skewing, and saturation effects. Moreover, this MEC model can be

coupled to a PWM inverter to include the switching effects. The details about this MEC modeling approach, and one form of such a model for a delta-connected squirrel cage induction machine are introduced in Chapter 3.

1.3 Thesis contribution

In this thesis, the fault associated with an open phase condition for a delta-connected induction machine is considered. One fault mitigation controller developed by Ahmed Sayed-Ahmed was added to the ac induction motor-drive system and is integrated into an MEC model for a delta-connected induction machine coupled to a PWM inverter. The whole system is simulated under both the open-loop and closed-loop motor-drive operating modes, under the aforementioned faulty condition. This is in order to verify the applicability and the validity of the introduced fault mitigation algorithm and accuracy of the global MEC model. The results obtained from the MEC model coupled to a PWM inverter are presented and compared to the results obtained from the TSFE model and the corresponding experimental setup which were given in an earlier reference [30]. Thus, these comparisons verify the validity of the modeling approach presented in this thesis for simulating such fault conditions.

1.4 Thesis organization

Including this introductory chapter, this thesis is organized in five more chapters. In the second chapter, basic principles and detailed explanations of the fault

mitigation method are reviewed and presented. In the third chapter, the MEC

modeling approach is explained with basic magnetic principles and a MEC model for

a 6 poles, 5-hp, delta-connected induction machine is given. In the fourth chapter, the

fault mitigation controller is added to the open-loop and closed-loop motor-drive

systems and connected to the MEC model and coupled to a PWM inverter. This

global model is used to simulate both the healthy and faulty operating conditions. The

simulation results are presented in the fifth chapter, and are compared to the results

obtained from the TSFE model and the corresponding experimental setup [30].

Finally, in the sixth chapter, conclusions and future work are presented.

Chapter 2
Analysis of Two-phase Mode of Operation of Delta-connected Motors

2.1 Introduction

As mentioned in the first chapter, delta-connected induction motors are not as widely used as wye-connected motors in the industrial and utility applications. Delta-connected induction motors are more common in high horsepower applications due to their special properties. Compared with wye-connected machines, delta-connected machines have less current in the stator phase windings, which means less ohmic losses and thermal stresses on the windings, which also means smaller frame sizes. Since the focus of this research was on a fault mitigation method and magnetic equivalent circuit (MEC) models for delta-connected induction motors, it was important to analyze the healthy three-phase mode of operation, and the faulty two-phase open-delta mode of operation of delta-connected induction motors under faulty condition, such as a short-circuit in one phase that has to be denergized. By comparing the stator resultant magneto-motive force (mmf) waveform and current space vector profile under the healthy three-phase mode of operation and the faulty two-phase open-delta mode of operation, the fault mitigation method can be explained in detail as given in the following sections.

In this chapter, the healthy three-phase mode of operation of a delta-connected induction motor and its drive system under normal healthy condition is analyzed and the expression of the stator resultant mmf is given in the first section. Then the two-phase open-delta mode of operation of the induction motor and its drive system is

illustrated in the second section. The expression of the stator resultant mmf under

faulty condition is given and compared with the expression under healthy three-phase

mode of operation, in order to best explain the key idea of the fault mitigation

algorithm from the mmf point of view. In the third section, the fault mitigation

algorithm is illustrated from the stator current space vector point of view. The

relationships of the phase currents and line currents under healthy condition and

faulty condition are compared and illustrated in the phasor diagram of section 2.3, see

Fig.2.3 [30].

2.2 Analysis of the healthy three-phase mode of operation of delta-connected induction motors

The three-phase circuit schematic of an inverter-fed induction motor with

delta-connected stator windings is depicted in Fig.2.1 [30].
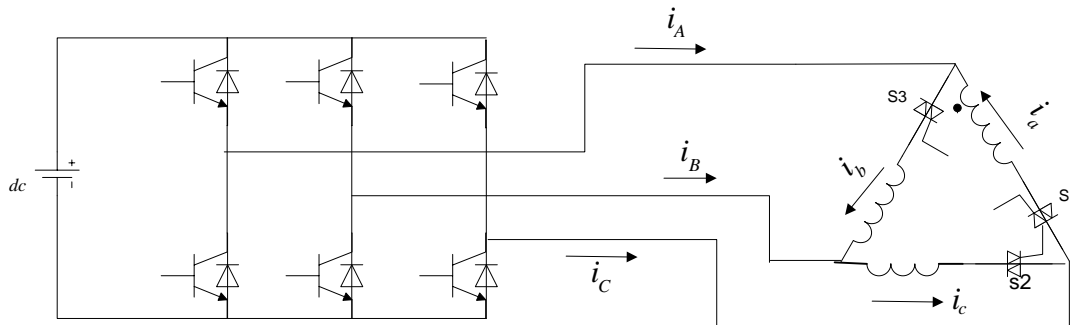
Fig. 2.1 Three-phase operation of a delta-connected induction motor-drive system

For a healthy three-phase mode operation of a delta-connected induction

motor-drive system, the motor line currents, i_A, i_B, i_C and the motor phase currents,

i_a, i_b, i_c have the following relationships:

$$i_a = I_{max} \cos(\omega t - \phi) \tag{2.1}$$

$$i_b = I_{max} \cos(\omega t - \phi - 2\pi/3) \tag{2.2}$$

$$i_c = I_{max} \cos(\omega t - \phi - 4\pi/3) \tag{2.3}$$

$$i_A = i_b - i_a \tag{2.4}$$

$$i_B = i_c - i_b \tag{2.5}$$

$$i_C = i_a - i_c \tag{2.6}$$

Where, ϕ is an arbitrary phase angle shift which will be explained later in order to explain the idea of the fault mitigation method used here for the two-phase open-delta mode of operation.

Accordingly, the stator magneto-motive force (mmf) for each phase of the stator winding can be expressed as follows [40]:

$$f_a = F_{max} \cos(\theta) \cos(\omega t - \phi) \tag{2.7}$$

$$f_b = F_{max} \cos(\theta - 2\pi/3) \cos(\omega t - \phi - 2\pi/3) \tag{2.8}$$

$$f_c = F_{max} \cos(\theta - 4\pi/3) \cos(\omega t - \phi - 4\pi/3) \tag{2.9}$$

where, F_{max} is the amplitude (peak) of the phase mmf [39].

Therefore, the stator resultant mmf MMF_s, can be expressed as follows [39]:

$$MMF_s = f_a + f_b + f_c = \frac{3}{2} F_{max} \left[\sin(\theta - \omega t) \right] \tag{2.10}$$

Hence, for a healthy three-phase delta-connected induction motor, the three phase currents are shifted by 120 electric degrees ($2\pi/3$ electrical radians) in the time domain and these phase currents produce a perfect rotating mmf waveform in the airgap of the delta-connected induction motors.

2.3 Analysis of the two-phase mode of operation of delta-connected induction motors

The two-phase mode of operation of an inverter-fed induction motor with delta-connected stator windings is depicted Fig.2.2 [30]. This kind of fault is common in industrial and commercial applications/utilities, and it may be caused by any accidental rupture in one of the motor phase windings, or a loose connection between the internal motor coils. These kinds of faults may cause great losses to industrial productivity and could threaten people's lives.
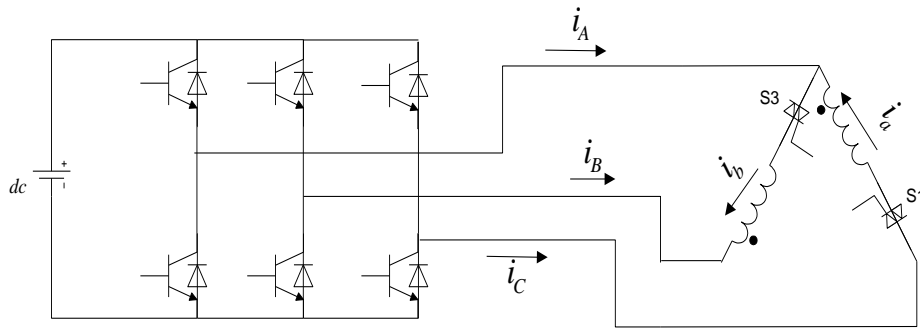
Fig.2.2 Two-phase operation of a delta-connected induction motor-drive system

For a two-phase mode of operation, that is an open delta-connected induction motor-drive system, the relationship between the motor line currents, i_A, i_B and i_C, and the motor phase currents, i_a, i_b and i_c, can be expressed as follows [30]:

$$i_a = I_{max} \cos(\omega t - \phi) \tag{2.11}$$

$$i_b = I_{max} \cos(\omega t - \psi) \tag{2.12}$$

$$i_c = 0 \tag{2.13}$$

$$I_A = i_b - i_a \tag{2.14}$$

$$I_B = -i_b \tag{2.15}$$

$$I_c = i_a \tag{2.16}$$

Where, ϕ and ψ are phase angles controlled by the motor's internal parameters and external terminal conditions and load, which will be explained later on. These angles are controllable through the inverter operation. Equations (2.11) through (2.16) showed that the phase currents have two degrees of freedom. Accordingly, the current in these two remaining active phases can be controlled independently. Presuming that phase c is the faulty phase, the mmfs produced by the healthy stator phases and their phase currents can be expressed as follows [30]:

$$f_a = F_{max} \cos(\theta)\cos(\omega t - \phi) \tag{2.17}$$

$$f_b = F_{max} \cos(\theta - 2\pi/3)\cos(\omega t - \psi) \tag{2.18}$$

$$f_c = 0 \tag{2.19}$$

Hence, the stator resultant mmf MMF_s, can be expressed as follows [30]:

$$MMF_s = f_a + f_b + f_c = \frac{1}{2}F_{max}\left[\cos(\theta - \omega t + \phi) + \cos(\theta - \omega t + \psi - 2\pi/3)\right]$$
$$+ \frac{1}{2}F_{max}\left[\cos(\theta + \omega t - \phi) + \cos(\theta + \omega t - \psi - 2\pi/3)\right] \tag{2.20}$$

The equation (2.20) showed that under the two-phase open-delta mode of operation, the stator resultant mmf MMF_s can be resolved into two main components. The first component was the forward mmf component and the second one was the backward mmf component. This backward stator mmf would be affecting the output torque adversely. A backward (negative/reverse) drag torque would be produced by the interaction between the backward component of the stator mmf and the backward component of the rotor mmf, and this drag torque decreased the net output torque. In addition, a substantial ripple in the torque time domain profile would be produced by the interaction between the backward component of the stator mmf and the forward

component of the rotor mmf, and the interaction between the forward component of the stator mmf and the backward component of the rotor mmf.

However, the magnitudes of both the forward and backward mmf components can be controlled by controlling the phase shift angles, ϕ and ψ, which have already been mentioned before. By controlling the angles, ϕ and ψ, such that $\psi - \phi = \pi/3 = 60°e$, the backward mmf component of the stator can be reduced to zero. This relationship can be verified mathematically as given next [30].

It follows from (2.20) that in order to eliminate the second term on the right hand side of that equation, that is the stator backward mmf, the following equation should be satisfied:

$$\cos(\theta + \omega t - \phi) = -\cos(\theta + \omega t - \psi - 2\pi/3) \tag{2.21}$$

From the trigonometric relation above, the following equation should be satisfied:

$$\theta + \omega t - \phi + \pi = \theta + \omega t - \psi - 2\pi/3 \tag{2.22}$$

Therefore, one must satisfy the following condition:

$$\psi - \phi = \pi/3 = 60°e \tag{2.23}$$

In this case, the stator resultant mmf of equation (2.20) can be rewritten as follows:

$$MMF_s = f_a + f_b + f_c = \frac{\sqrt{3}}{2} F_{max} \left[\sin(\theta - \omega t)\right] \tag{2.24}$$

Inspection of equation (2.24) shows that if the stator backward MMF was eliminated, the machine will only have a stator resultant mmf that rotates in the forward direction, even under this two-phase mode of operation. Comparison between

equation (2.24) and equation (2.10) shows that under the two-phase open-delta mode

of operation, with the stator backward mmf being eliminated, the magnitude of the

remaining two active phase currents should be increased by a factor of $\sqrt{3}$ in order to

maintain the same stator mmf amplitude existing in the airgap under normal healthy

condition. Therefore, under such condition, the machine produces a near perfect

rotating mmf in the airgap even under the two-phase open-delta mode of operation.

2.4 Analysis of the fault mitigation strategy

In the previous two sections, the healthy three-phase mode of operation and

the two-phase open-delta mode of operation conditions have been analyzed. In a

delta-connected motor-drive system, when one of the motor phases is disconnected,

the currents flowing through the remaining two active phase windings are highly

unbalanced. Also, the stator resultant mmf is dependent on the phase shift between

the currents flowing through the other two healthy phase windings as was

demonstrated in the previous sections, which can be seen from equations (2.17)

through (2.20). Therefore, the introduced fault mitigation strategy is mainly to control

the two active motor line currents in order to produce a near perfect rotating mmf

with only a forward direction. This is achieved by forcing the stator backward mmf

component to, or at least close to, zero. This can also be shown in space vector

notations as follows [41]:

$$MMF_s = \frac{3}{2} NK_w \vec{i_s} \tag{2.25}$$

where, $\vec{i_s}$, is the space vector of the stator currents, and it can be expressed in

terms of the three phase currents and the complex operator, $\alpha = 1\angle 120^\circ e = \mathrm{e}^{+j\frac{2\pi}{3}}$, as

follows [41]:

$$\vec{i_s} = i_a + \alpha i_b + \alpha^2 i_c = I_s \mathrm{e}^{i(\omega t - \theta)} = I_{\max} \mathrm{e}^{i(wt - \theta)} \tag{2.26}$$

When one of the phases is disconnected, the stator current space vector can be

decomposed into a forward component, $\vec{i_{sf}}$, and a backward component, $\vec{i_{sb}}$, as

follows [30]:

$$\vec{i_s} = \vec{i_{sf}} + \vec{i_{sb}} \tag{2.27}$$

Therefore, the stator resultant mmf that corresponds to these current

components can be expressed as follows [30]:

$$MMF_s = \frac{3}{2} NK_w \vec{i_{sf}} + \frac{3}{2} NK_w \vec{i_{sb}} \tag{2.28}$$

Equation (2.28) shows that the stator resultant mmf can also be decomposed

into two components in terms of stator current space vectors. The first component is

the forward component of the stator mmf and the second one is the backward

component of the stator mmf. The backward mmf component of the stator can be set

to zero by controlling the angles ϕ and ψ such that $\psi - \phi = \pi/3 = 60^\circ e$, which was

already discussed in the previous section.

In any three phase motor-drive system, besides the reference signals, the three

phase line currents can be measured as feedback signals to the controller. If the three

line currents were measured and transferred to a synchronous reference frame rotating

backward in a clockwise direction, which rotated at a speed equal to the synchronous

speed, the backward components of the stator current space vector would appear as a dc value along both the d-axis and the q-axis, and the forward counter-clockwise component of the stator current space vector would appear as an ac component with a frequency equal to double the line frequency. In order to force the two dc values in d-axis and q-axis to zero so as to eliminate the backward component of the stator mmf, two PI controllers were added on the d-axis and the q-axis under a synchronously rotating clockwise frame of reference. On the other hand, a low pass filter can be added under the synchronously rotating clockwise frame of reference in order to eliminate the high frequency of the ac values.

When the machine was running under a healthy three-phase mode of operation, the backward component of the stator current space vector was almost zero. In this case, the two dc components of the stator current space vector in the synchronously rotating clockwise frame of reference were also almost zero. Hence, the fault mitigation controller output was negligible to the motor-drive system under the healthy conditions. On the other hand, when the machine was running under a two-phase open-delta mode of operation, the backward component of the stator current space vector had a significant value. Then the backward component appeared as two dc components, one on the d-axis and the other on the q-axis in a clockwise synchronously rotating frame of reference. Hence, the fault mitigation controller forced the two dc values to zero. Therefore, the backward component of the stator current space vector was set to zero and this resulted in a set of almost balanced line currents with equal magnitudes and inter-phase shift angles of $120^{\circ} e$ [30]. At the same time, the remaining two active phase currents were rendered with equal

magnitudes and a phase shift angle of $60°e$, which lead to only a counter-clockwise synchronously rotating mmf component. Hence, the overall result was a set of motor terminal line currents, i_A, i_B and i_C, that were balanced with a sequential phase shift of $120°e$, which resulted in a balanced positive sequence set of three phase currents.

The relationship between the motor line current phasors, $\overline{I_A}$, $\overline{I_B}$, $\overline{I_C}$, and phase current phasors, $\overline{i_a}$, $\overline{i_b}$, $\overline{i_c}$, for the two-phase open-delta mode of operation is illustrated in the phasor diagram of Fig.2.3. The green phasors stand for the line currents under healthy condition and the red phasors stand for the phase currents under two-phase open-delta mode of operation with the activated fault mitigation controller. When the machine was running under the healthy three-phase mode of operation, there was a set of balanced line currents, $\overline{I_A}$, $\overline{I_B}$, and $\overline{I_C}$. When the machine was running under the two-phase open-delta mode of operation, there were only two phase currents, $\overline{i_a}$ and $\overline{i_b}$, and they had a phase shift angle between them of $60°e$. The fault mitigation controller can use the two phase currents, $\overline{i_a}$ and $\overline{i_b}$, to generate a near perfect rotating mmf waveform in the airgap of the machine and produced three "almost balanced" line currents, $\overline{I_A}$, $\overline{I_B}$ and $\overline{I_C}$, which are shown in Fig. 2.3 [30].
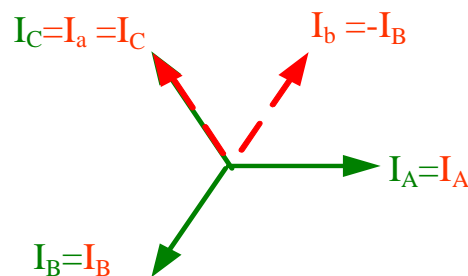
Fig.2.3 Phasor diagram of the motor line and phase currents under the two-phase mode of operation

Chapter 3
The Magnetic Circuit Modeling Approach

3.1 Introduction

Numerous induction machine models have been developed in the past few years [42]. These different kinds of induction machine models include the simple T-Equivalent Circuit models [43], Coupled Circuit models [44], Magnetic Equivalent Circuit models [35], and Finite Element models [45]. The differences between these models include the level of desired accuracy, execution time, and the complexity of the physical phenomena that need to be considered in the model. Accordingly, under different considerations and requirements, different models should be used.

The T-Equivalent circuit models are widely used in the ac drive industry. This wide use of this type of method is due to its simplicity, fast execution time and relatively good accuracy. The fast execution time is a very important aspect in real-time motor control systems applications because it facilitates the use of this type of model in digital microprocessor-based control of these ac motor-drive systems. Moreover, the parameters of this model can not only be calculated from knowledge of the particulars of a given ac induction motor design, but also can be measured by standard blocked rotor and no-load (open circuit) motor tests [46], which can provide more accurate parameters. It should be pointed out that the T-Equivalent circuit model can only be used to simulate the machine under steady state operating conditions. However, if the starting transient response and sudden load change response should be sought and accurate dynamic performance solutions need to be provided, the T-Equivalent circuit models cannot provide such accurate dynamic

performance results. Therefore, a more accurate dynamic model should be used for such type of applications. Thus, the well-known state-space coupled circuit models [44] in the natural a-b-c frame of reference can be used here to provide accurate dynamic performance results including the effects of space harmonics due to the stator and the rotor windings' layouts in such machines. There are two different sets of key parameters that exist in such state-space dynamic models of such machines. One set of parameters is the time-varying mutual inductances between the stator and the rotor circuits, and these parameters are updated constantly in the simulation/computation process. The other set of parameters is the self inductances of both the stator and rotor windings [47]-[49]. One well-known model that can be derived from the aforementioned natural a-b-c frame of reference state-space coupled circuit model is the coupled circuit flux-linkage and/or current frame of reference state-space model formulated in the d-q-o frame of reference.

In addition to these models, there are two more models that were used to simulate the dynamics of the induction motors and were compared in this thesis. Namely these are the Magnetic Equivalent Circuit (MEC) model in the natural a-b-c flux-linkage frame of reference and the Time-Stepping Finite Element (TSFE) model which is also inherently set in the natural a-b-c frame of reference. The MEC model allows one to incorporate space-harmonics due to the discrete winding distribution, stator and rotor slotting, as well as the saliency effect caused by saturation of the magnetic material in the core of a given machine. Moreover, the squirrel-cage deep-bar effect, also known as the skin effect, can be included in such a model to provide a more realistic starting transient simulation and response for such machines [50]. The

TSFE model can provide the opportunity for obtaining the most accurate results, in

comparison with all the other aforementioned models. However, the execution time

for a TSFE based simulation is much longer than all the other models due to TSFE

model complexities.

In this chapter, the development and formulation of the MEC model are

briefly introduced and the formulation of the MEC model for a delta-connected 5-hp

squirrel cage induction machine is illustrated in detail. This is followed by the

implementation of the MEC model for the 5-hp motor-drive system subject of this

thesis, which is discussed in detail below.

3.2 Magnetic equivalent circuit method

The concept of magnetic circuits has been widely used in the design of

electromagnetic devices in industry, and this concept is based on the analogy between

magnetic and electric circuits based on Kirchhoff's Laws, as applied in electric circuit

theory. The formulation of the MEC model is based on the integral form of

Maxwell's equations:

$$\oint \vec{H} \cdot d\vec{l} = I_{enclosed} \tag{3.1}$$

$$\oint_S \vec{B} \cdot d\vec{s} = 0 \tag{3.2}$$

$$\oint \vec{E} \cdot d\vec{l} = -\frac{\partial}{\partial t}(\int \vec{B} \cdot d\vec{s}) \tag{3.3}$$

These three equations above are named as Ampere's Law, Gauss's Law for

Magnetism, and Faraday's Law, respectively. The magnetic flux density, $\vec{B}$, magnetic

field density, $\overline{H}$, electric field intensity, $\overline{E}$, and current density $\overline{J}$ are related by the constitutive relations as the follows:

$$\overline{B} = \mu \overline{H} \tag{3.4}$$

$$\overline{J} = \sigma \overline{E} \tag{3.5}$$

Where, μ , is the magnetic permeability of the medium, and, σ , is the electric conductivity of the medium. The MEC model development given next is based on the magnetic field formulations given above in equations (3.1) to (3.5), from which magnetic reluctances, $\mathcal{R}$, and permeances, $\mathcal{P}$, are derived.

In this thesis, the development of an MEC model for a 5-hp squirrel-cage induction machine, the cross-section of which is given in Fig.3.1 [38], is being considered. This machine has 6 poles, 36 stator slots and 45 rotor slots. It has a double-layer stator winding with a layout as shown in Fig.3.2 [38]. This machine has two coils per pole per phase, a total of 36 coils, with 20 turns per coil. In Fig.3.2, "Top" referred to the coil side/part of the stator slot closest to the air gap, whereas "Bottom" referred to the coil side/part of the stator slot closest to the back iron. In addition, the magnetic equivalent circuit of the stator slot with such a double-layer winding is depicted in Fig.3.3 [38]. In this magnetic equivalent circuit representation, $\mathcal{R}_{S_{TAN^i}}$, is the tangential leakage reluctance of the inner (Bottom) stator winding layer and, $\mathcal{R}_{S_{TAN^o}}$, is the tangential leakage reluctance of the outer (Top) layer of the stator winding. Meanwhile, the teeth of the stator are divided into two reluctances, $\mathcal{R}_{S_{TOOTH^i}}$, for the inner (Bottom) of the stator winding part of the tooth and, $\mathcal{R}_{S_{TOOTH^o}}$, for the lower (Top) part of the tooth. Moreover, the effect of the current carried by every coil

side in the slot can be accounted for by the mmf sources, which can be seen in Fig.3.3. Here, $\mathcal{F}_{Si}$, is the mmf produced by the coil side in the inner (Bottom) layer whereas, $\mathcal{F}_{So}$, is the mmf produced by the coil side in the outer (Top) layer. The back iron can be characterized by a single reluctance value, $\mathcal{R}_{S_{YOKE}}$. The index m is being used to distinguish between the individual stator tooth reluctances.

The magnetic equivalent circuit of the stator slot described above can be further simplified as depicted in Fig 3.4 [38]. In this magnetic equivalent circuit, every tooth can be represented as a single tooth reluctance, $\mathcal{R}_{S_{TOOTH}}$, and a single mmf source, $\mathcal{F}_{s}$. In addition, the stator slot tangential leakage reluctance can be also simplified to a single reluctance term, $\mathcal{R}_{S_{TAN}}$, and this tangential leakage reluctance of the slot is only a function of the machine slot geometry [50] and the value of this slot tangential leakage reluctance is not changing during machine operation. In this magnetic circuit representation of the stator slot it is assumed that the magnetic flux flow in either of the two directions, namely, radial and/or tangential, which can be seen in Fig.3.4. The mmf sources were placed in the stator teeth in order to represent the effect of the current carrying coil sides.

The squirrel-cage rotor slot design of this machine was typical of induction machines that can provide good rated load performance, such as high power factor, high efficiency and low slip at rated load. On the other hand, it can provide an acceptable starting performance such as high starting torque, low starting current, etc. This is due to the deep-bar rotor slot design, which provided an increase of rotor impedance/resistance at starting, hence, increasing the starting torque and reducing

the starting current, while also providing low rotor impedance/resistance at rated conditions resulting in relatively good performance at rated load conditions [40]. This was due to the so-called deep bar effect, also known as skin effect. This deep-bar effect resulted in the increase of the rotor impedance/resistance at starting when the frequency of rotor currents is high. Meanwhile, the rotor impedance decreases, as the rotor speed approached the synchronous speed, because of the corresponding decrease of the frequency of rotor currents. This variation of the rotor impedance has to be accounted for in the model if it is required to provide an accurate solution of the transient operation of the machine.
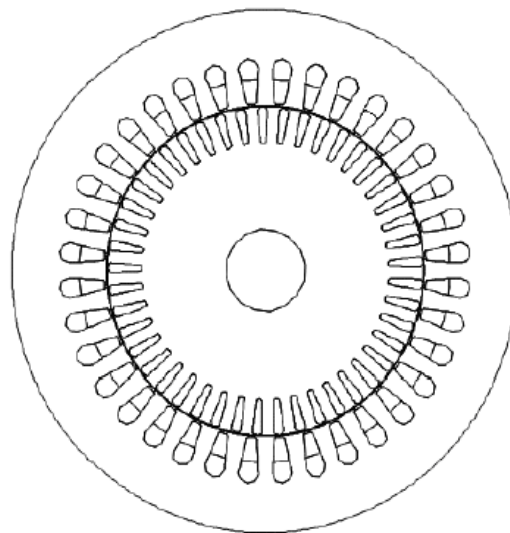
Figure 3.1 Stator slots of the 5-hp squirrel-cage induction machine

Top	A+	C-	C-	B+	B+	A-	A-	C+	C+	B-	B-	A+	A+	C-	C-	B+	B+	A-
Bottom	A+	A+	C-	C-	B+	B+	A-	A-	C+	C+	B-	B-	A+	A+	C-	C-	B+	B+
Slot	1	2	3	4	5	6	7	8	9	10	11	12	13	14	15	16	17	18

	A-	C+	C+	B-	B-	A+	A+	C-	C-	B+	B+	A-	A-	C+	C+	B-	B-	A+
	A-	A-	C+	C+	B-	B-	A+	A+	C-	C-	B+	B+	A-	A-	C+	C+	B-	B-
	19	20	21	22	23	24	25	26	27	28	29	30	31	32	33	34	35	36

Figure 3.2 Rotor slots of the 5-hp squirrel-cage induction machine
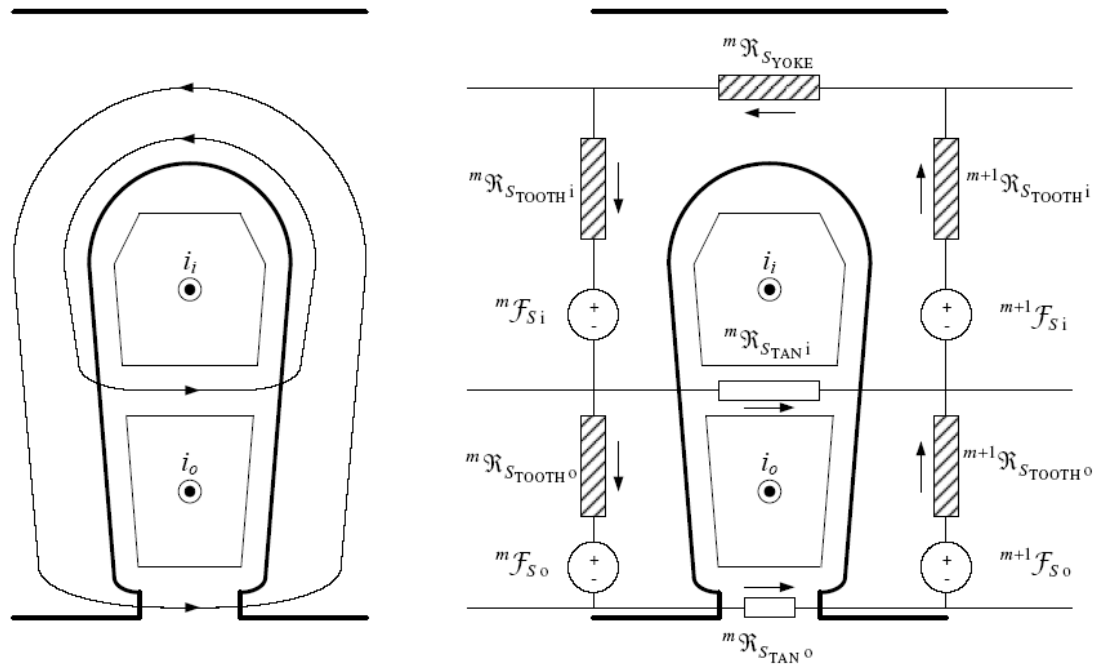
Figure 3.3 MEC representation of a double-layer stator winding
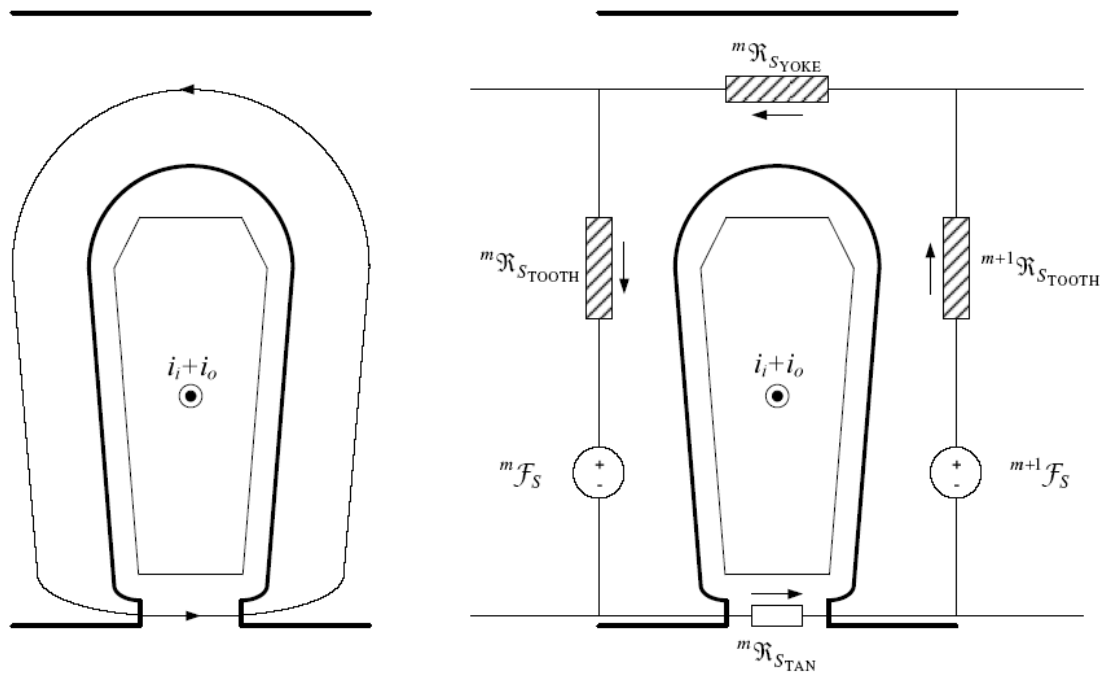
Figure 3.4 Simplified MEC representation of a double-layer stator winding

However, in this thesis, a simplified rotor slot magnetic equivalent circuit model was used without considering the deep-bar effect which is depicted in Fig. 3.5 [38]. This model of the rotor slot does not allow one to directly incorporate the deep-bar effect in the magnetic circuit-electrodynamics solution of the starting performance of the machine. So far, both the stator and rotor slot magnetic equivalent circuits have been defined under this approximation and the global MEC model of the induction machine can now be assembled. This global model, a portion of which is depicted in Fig.3.6 [38]. In this figure, air gap reluctances were included to provide the coupling between the rotor and the stator magnetic circuits. The stator and rotor coupling in the MEC model was accomplished in such a manner that every tooth on the stator was coupled to every tooth on the rotor, and vice versa. More details about this MEC model of this type of induction machine can be found in the work of Sizov [38].

The complete MEC model representation of the squirrel-cage induction machine including the interaction of electric, magnetic, and mechanical systems is shown in the functional block diagram of Fig.3.7 [38]. There were four inputs from the electrical system into the MEC block, namely, three stator flux linkages and a vector of N_R rotor flux linkages. Moreover, the MEC block has four electrical outputs, namely, three stator phase currents and one vector of N_R rotor currents. Here, it should be reiterated that the N_R was the number of rotor slots, which was also the number of bars and current loops in the rotor cage/winding. The derivatives of the stator fluxes (flux linkages) can be obtained from the stator electric equivalent circuits, such that the stator flux can be calculated by integration of the obtained derivatives of the stator flux, $\dot{\lambda}_a$, $\dot{\lambda}_b$ and $\dot{\lambda}_c$, respectively. Hence these stator fluxes (flux linkages)

were used as the input to the MEC portion of the global model. In the MEC portion of

the global model, the stator currents and rotor currents were calculated and fed back

to the electric equivalent circuit of the stator as inputs. Furthermore, the MEC portion

of the global model was also coupled to the mechanical system through its output

torque, T_{em}, and the rotor position feedback angle, θ_R, which can be clearly seen in

the functional block diagram of Fig 3.7 [38].
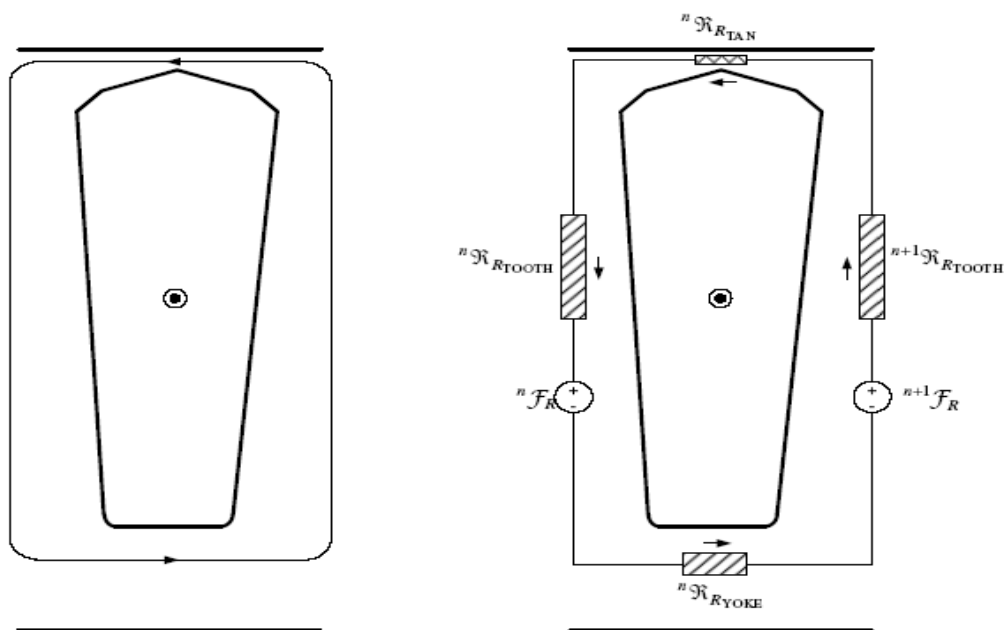
Figure 3.5 Simplified MEC representation of a rotor slot winding
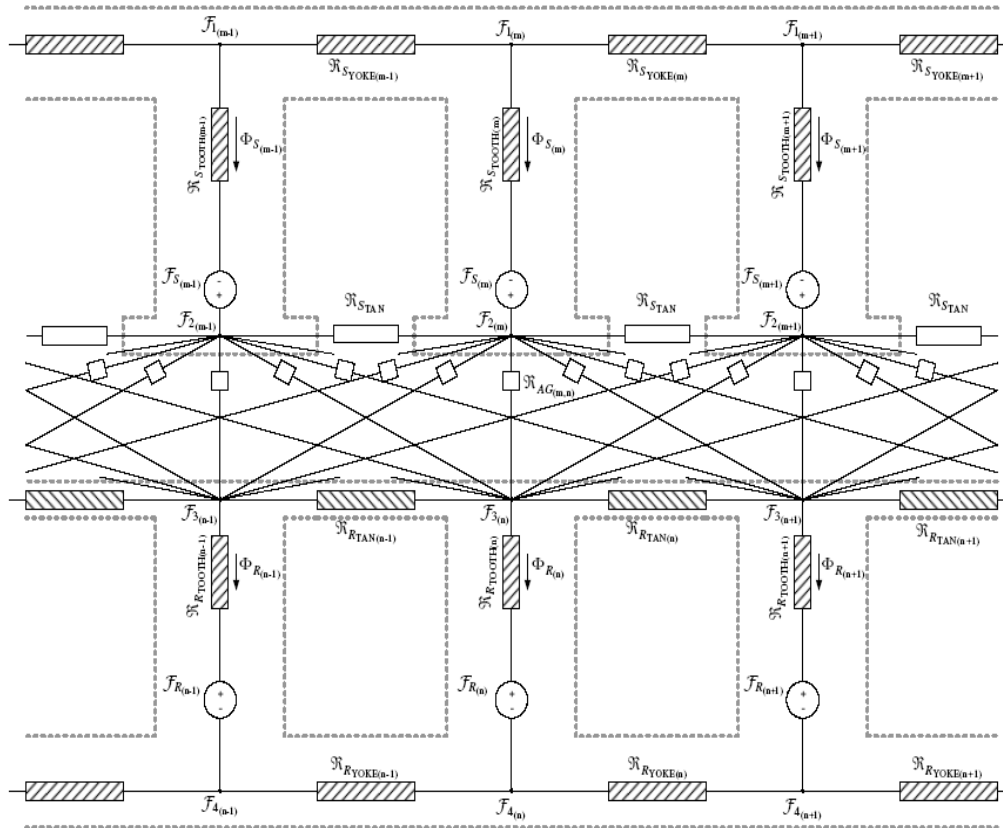
Figure 3.6   MEC representation of a 5-hp delta-connected induction motor
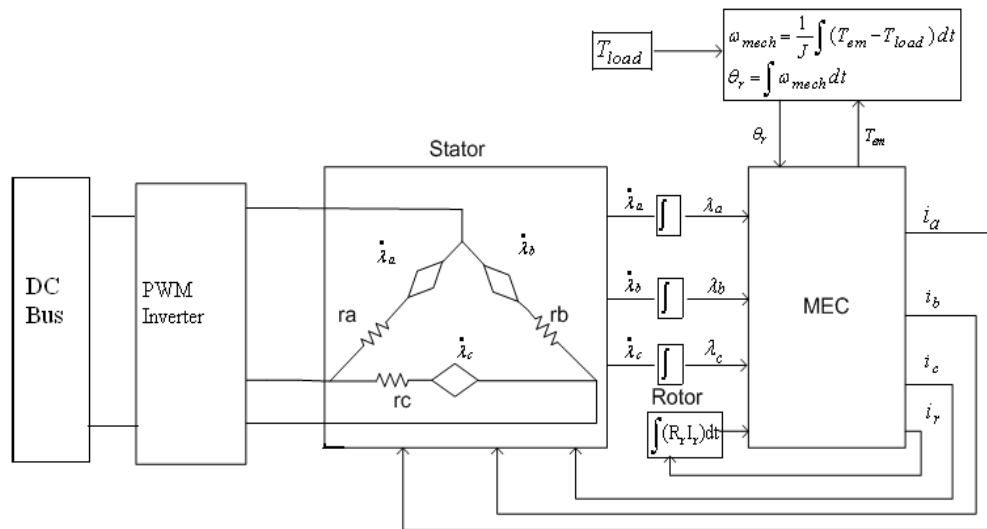
Figure 3.7   Block diagram of a complete squirrel-cage delta-connected induction
motor MEC model and its drive system

In Sizov's previous work [38], it was already verified that the global MEC model of very similar nature to what has been described here can provide accurate results with far less execution time compared to the TSFE approach in the simulation of the performance of polyphase squirrel-cage induction machines, including cases with faults in the stator and rotor electric circuits. In the next chapter, the global MEC model will be linked to a controller with fault mitigation capabilities containing a PWM inverter. This was carried out in order to verify the fault mitigation control algorithm, and verify the validity of the global MEC model in simulating such motor-drive systems operating under partial-fault conditions. This constituted the main contribution of this thesis. This is intended for emergency "limp-home" applications for various industrial systems.

Chapter 4:
Linking the Magnetic Circuit Model to Matlab-Simulink to Form the Global Model for Open-Loop and Closed-Loop Operation of Open-Delta Motors

4.1 Introduction

Open-loop and closed-loop Adjustable Speed Drives "ASDs" have been widely used in many industrial and commercial applications. For the open-loop type, the control of most of these drives is mostly based on the conventional scalar constant volts-per-hertz (V/f) control method, and in the closed-loop type a vector control/field oriented control approach is used. The simple open-loop volts-per-hertz (V/f) control is a common drive control method, where the motor voltage, V, is adjusted proportionally to the stator current frequency, f. It can provide a smooth speed-torque control over a wide dynamic range and at the same time, reduce the complexity of the system. Nevertheless, one disadvantage of such a drive system is that the developed torque cannot be controlled directly. In addition, the reliability and performance quality of this motor-drive system remains a significant concern, especially in critical applications under partial fault conditions. Accordingly, in such applications the closed-loop vector-controlled motor-drive control system approach is the preferred choice.

The main advantage of the closed-loop vector-controlled motor-drive system is that it can decouple the motor flux and the motor torque such that each of them can be controlled independently. As previously mentioned, this control strategy is also known as the field oriented control approach. The three phase a, b, and c current phasors in the a-b-c frame of reference are transformed to a d-q-o frame of reference,

that is the so-called d-q synchronously rotating reference frame using the well known

Park's transformation [40]. Here, the d-axis component of the stator current

represents the flux producing component of that current and the q-axis component of

the stator current represents the torque producing component of that current. These

two decoupled d and q current components can be independently controlled using two

separate PI controllers. The outputs of the PI controllers are transformed back to the

a-b-c frame of reference using the inverse of Park's transformation. This unique

capability of dealing with a d-axis current component/flux and a q-axis current

component/flux enables the induction motor-drive system to replicate the unique

torque production and torque-speed performance of a DC motor with a separate field

excitation.

In this chapter, the basic principles of the conventional scalar/constant volts-

per-hertz (V/f) control approach are briefly reviewed, and then the concept of the

fault mitigation strategy for the open-loop drive system is discussed. After that, the

principles of the closed-loop vector control motor-drive system approach, and the

fault mitigation strategy for it are presented. Finally, both the open-loop and the

closed-loop systems with two respective fault mitigation controllers are linked to the

MEC motor model in a Matlab-Simulink environment and simulated under a healthy

condition and a faulty condition.

4.2 Basic principles of the conventional scalar constant (V/f) control approach

As mentioned earlier, scalar constant (V/f) control is widely implemented in

motor-drive systems due to its simplicity. The main principle is to maintain a constant

ratio between the voltages applied at the motor terminals and the stator voltage and

current frequency. This is a very popular control method for low-cost drives such as low-horsepower pumps and fans. The relationship between the stator induced emf and machine airgap flux can be expressed as follows [52]:

$$E = 4.44 N f \phi K_w \qquad (4.1)$$

where, E is the induced emf in the stator per phase (line to neutral).

N is the number of series turns per phase.

ϕ is the resultant air gap flux per pole.

f is the frequency of the energy source.

K_w is the stator winding factor, which includes distribution, pitch and skewing effects.

Inspection of equation (4.1) shows that the ratio between the stator induced emf and the supply frequency can be expressed as follows:

$$\frac{E}{f} = 4.44 N \phi K_w \qquad (4.2)$$

In addition, the relationship between the applied phase voltage and the induced emf in the stator winding can be expressed as follows:

$$\bar{E} = \bar{V} - \bar{I}(r + jx_l) \qquad (4.3)$$

where, $\bar{E}$, is the corresponding phasor of the induced emf per phase, and, $\bar{V}$, is the motor's applied voltage per phase. Here, r and x_l, are the stator resistance and the leakage reactance in ohms per phase, respectively.

When the machine runs under high speed condition (light load or no-load), the voltage drop across the stator resistance and the leakage reactance is insignificant and can be neglected. However, the voltage drop cannot be neglected when the machine

runs under low speed (heave load) condition. In such case, this voltage drop should be compensated for in order to maintain the same airgap flux in the machine under a constant (V/f) approach. Therefore, the motor speed can be fully controlled by controlling the magnitude of the applied supply voltage and the corresponding supply frequency. A set of torque-speed curves is depicted in Fig. 4.1 at different supply voltages and frequencies such that (V/f) is constant. One should notice that the maximum (or breakdown) torque remains nearly the same for these various values of voltages and frequencies.
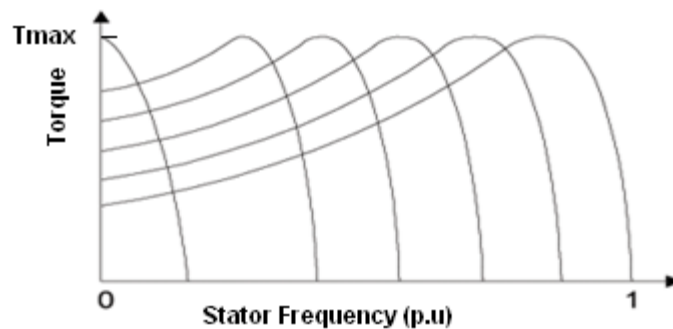
Figure 4.1 Torque–speed characteristics at variable frequencies

4.3 Analysis of the open-loop drive system including a fault mitigation controller under two-phase operation of a delta-connected induction motor

The fault mitigation algorithm has already been explained in Chapter 2. In the case of the open-delta mode of operation, the stator current space vector can be decomposed into two components, namely the backward clockwise rotating stator current space vector and the forward counter-clockwise rotating stator current space vector. In a motor-drive system, if the motor line currents are measured and transferred to a synchronous reference frame rotating backward in a clockwise direction at a speed equal to the synchronous speed, the backward component of the

stator current space vector appears as a dc value in both the d-axis and the q-axis, and to this clockwise rotating reference frame the forward counter-clockwise component of the stator current space vector appears as an ac component with a frequency equal to double the line frequency. Here, these dc values can be forced to zero by the two d-axis and q-axis PI controllers to eliminate the backward component of the stator mmf, and the double frequency ac component due to the forward rotating current space vector is filtered through a low pass filter. The diagram of the open-loop scalar constant (V/f) control including the fault mitigation controller is shown in Fig.4.2 [30].

The solid-line parts in the diagram stand for the open-loop motor-drive system and the dashed-line parts stand for the fault mitigation controller. For any conventional open-loop scalar constant (V/f) control, the ratio between the voltage and the frequency of the reference signal fed to the modulator is kept constant. This is the main control signal of the open-loop motor-drive system. For the fault mitigation controller, the three motor line currents are measured and transferred to a synchronous reference frame rotating backward in a clockwise direction at a speed equal to the synchronous speed, while the double-frequency ac components are filtered through the low pass filter (LPF), and the values of the dc components are forced to zero by the two current PI controllers. After this, the fault mitigation controller signal is transferred back to the a-b-c reference frame and added to the main control signal of the motor-drive system. This signal is sent to the modulator to generate the corresponding PWM signals to control the motor [30].

The simulink model of the controller is shown in Fig.4.3. The sampling

frequency was 5K Hz which was set to be the same as the sampling frequency of the

real-time Digital Signal Processor used in the drive system. This was in order to

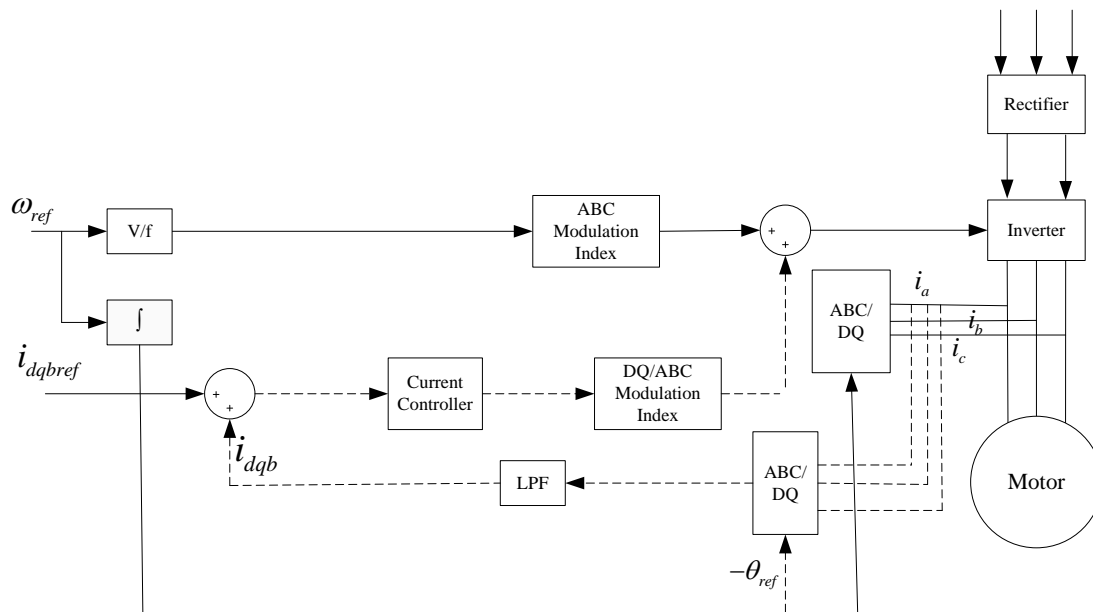consistently compare the simulation results with the experimental results.

Fig.4.2 Open-loop scalar constant (V/f) control including the fault mitigation
controller

The entire open-loop motor-drive system including the fault mitigation

controller, which is linked to the MEC model, implemented in a Matlab-Simulink

environment is shown in Fig.4.4.

As mentioned in Chapter 3, the MEC model can provide accurate results with

far less execution time compared with the TSFE method. The control signal was

converted to switching commands to the power switches in the inverter bridge using

PWM techniques. Then the inverter bridge was connected to the MEC model. The

time-step of the simulation for the MEC model and the inverter bridge were chosen to

be equal to one micro-second (1×10^{-6} second), which was the same as in the TSFE

model. The sampling time of the controller was chosen to be equal to 200 micro-

seconds to replicate the implementation in the DSP chip used in the experimental

work. Hence, a rate transition block was required between the MEC model and the
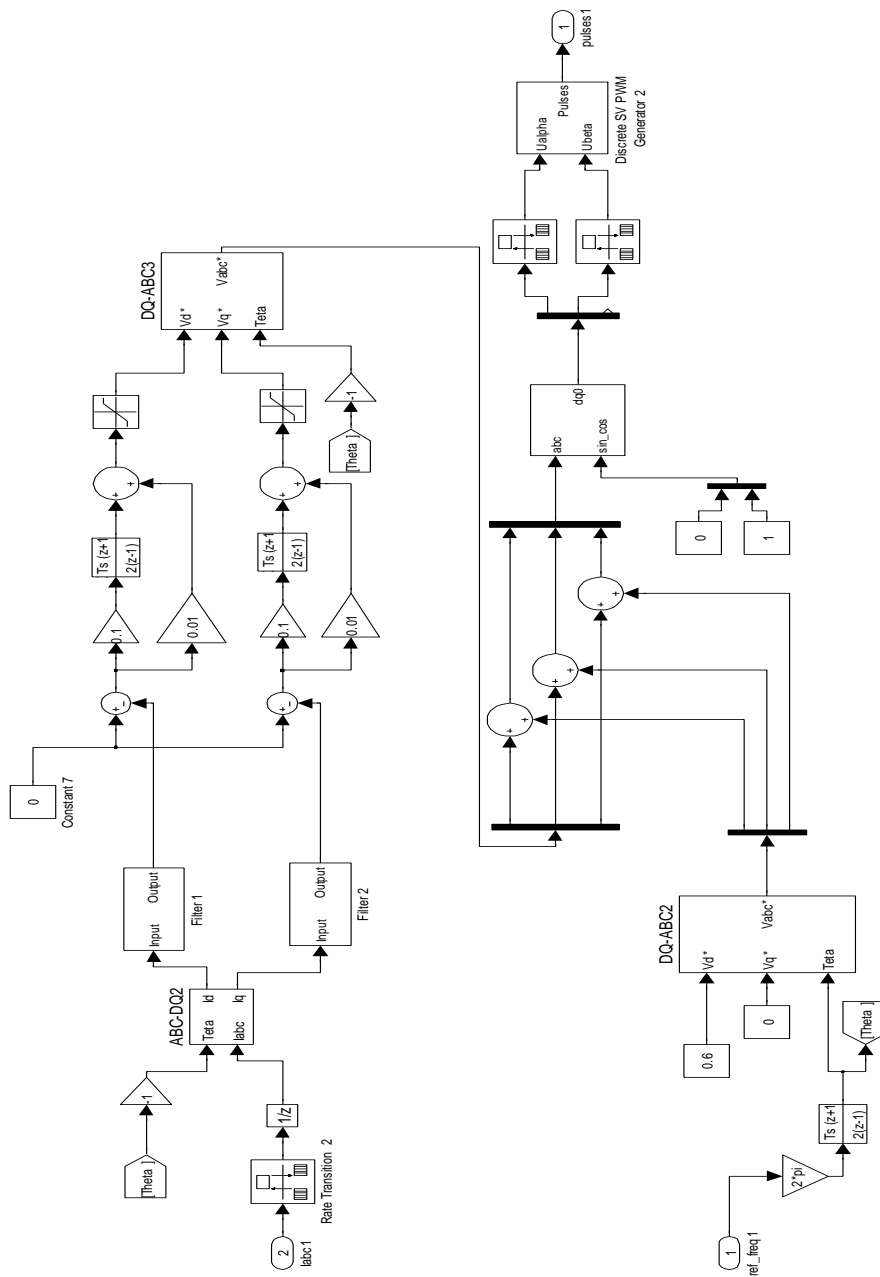
controller, see Fig.4.4.

Fig.4.3 Simulink block diagram of the open-loop scalar (V/f) control including the
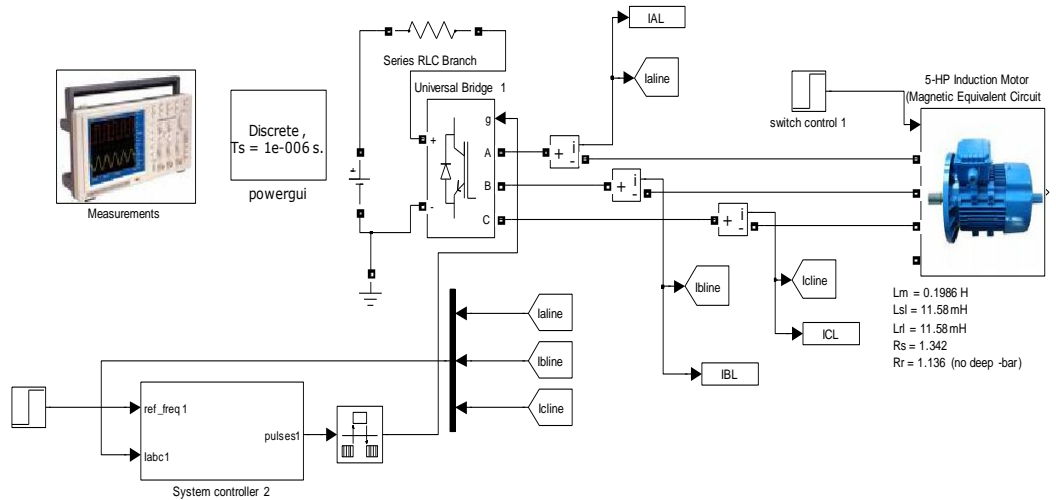fault mitigation controller

Fig.4.4 The entire open-loop motor-drive including the fault mitigation controller implemented in Matlab-Simulink environment

4.4 Basic principles of the closed-loop vector control approach

In a separately excited dc machine, the motor torque and the motor flux can be controlled independently. The developed torque, neglecting the armature reaction effect, can be expressed in terms of the machine design constant, K, the armature current I_a, and the field current, I_f as follows [52]:

$$T = KI_aI_f \tag{4.4}$$

Hence, the motor's developed torque is a function of the armature current, I_a, and the field current, I_f. If the field current is kept constant, it follows that the motor's developed torque is adjusted by controlling the armature current. Hence, in the torque production process, the motor flux (field current) and armature current are completely decoupled, that is both are independent of each other. This type of motor has been demonstrated to provide an excellent torque and speed control performance under both transient and steady state operations.

The purpose of the closed-loop vector control induction motor-drive system is to emulate/replicate the excellent speed and torque control performance of the above mentioned separately excited dc motor-drive system. This can be achieved by transforming the motor equations into a suitable synchronously rotating frame of reference in which the sinusoidally varying variables appear as dc components. It is also required to decouple the current component establishing by the flux from the current component producing the torque in this synchronously rotating frame of reference, which is established here for motor current representation. The basic equations for a three-phase induction motor in a synchronously rotating frame of reference can be expressed as given below.

For the stator in the d-q frame of reference one can write [52]:

$$v_d^e = R_s i_{ds}^e + \frac{d\psi_{ds}^e}{dt} - \omega_e \psi_{qs}^e \tag{4.5}$$

$$v_q^e = R_s i_{qs}^e + \frac{d\psi_{qs}^e}{dt} + \omega_e \psi_{ds}^e \tag{4.6}$$

For the rotor in the d-q frame of reference one can write [52]:

$$0 = R_r i_{dr}^e + \frac{d\psi_{dr}^e}{dt} - (\omega_e - \omega_r)\psi_{qr}^e \tag{4.7}$$

$$0 = R_r i_{qr}^e + \frac{d\psi_{qr}^e}{dt} + (\omega_e - \omega_r)\psi_{dr}^e \tag{4.8}$$

where, v_d and v_q, are the d and q voltage components in the synchronously rotating frame of reference. Here, R_s, is the stator resistance. Meanwhile, i_{ds} and i_{qs}, are the d and q stator current components in a synchronously rotating frame of reference, while, ψ_{ds} and ψ_{qs}, are the d and q stator flux components in the

synchronously rotating frame of reference. Meanwhile, ω_e, is the motor synchronous speed, while, R_r, is the rotor resistance. Furthermore, i_{dr} and i_{qr}, are the d and q rotor current components in synchronously rotating frame of reference, while, ψ_{dr} and ψ_{qr}, are the d and q rotor flux components in the synchronously rotating frame of reference. Meanwhile, ω_r, is the motor (rotor) speed.

In this frame of reference, the developed machine torque can be expressed as follows [52]:

$$T = (3/4)P(L_m/L_r)(i_{qs}^e\psi_{dr}^e - i_{ds}^e\psi_{qr}^e) \tag{4.9}$$

where, L_m, is the stator/rotor mutual inductance, and L_r, is the rotor self inductance. Meanwhile, P, is the number of the motor poles.

In addition, the rotor current components can be related to the rotor flux and stator current components as follows [52]:

$$i_{dr}^e = \psi_{dr}^e/L_r - L_m/L_r i_{ds}^e \tag{4.10}$$

$$i_{qr}^e = \psi_{qr}^e/L_r - L_m/L_r i_{qs}^e \tag{4.11}$$

Substituting (4.10) and (4.11) into (4.5) to (4.8) results in the following:

$$\frac{d\psi_{dr}^e}{dt} + \frac{R_r}{L_r}\psi_{dr}^e - \frac{L_m R_r}{L_r}i_{ds}^e - (\omega_e - \omega_r)\psi_{qr}^e = 0 \tag{4.12}$$

$$\frac{d\psi_{qr}^e}{dt} + \frac{R_r}{L_r}\psi_{qr}^e - \frac{L_m R_r}{L_r}i_{qs}^e + (\omega_e - \omega_r)\psi_{dr}^e = 0 \tag{4.13}$$

If the synchronously rotating frame of reference is particularly chosen with angular orientation such that the resultant rotor flux is aligned along the d-axis, it

follows that $\psi_{qr}^e = 0$, and also $\dfrac{d\psi_{qr}^e}{dt} = 0$. Consequently, equation (4.12) and

(4.13) can be simplified to the following [52]:

$$\frac{d\psi_{dr}^e}{dt} + \frac{R_r}{L_r}\psi_{dr}^e = \frac{L_m R_r}{L_r} i_{ds}^e \qquad (4.14)$$

$$\omega_e = \omega_r + \frac{L_m R_r}{L_r} \frac{i_{qs}^e}{\psi_{dr}^e} \qquad (4.15)$$

In addition, the torque equation (4.9) can be simplified and rewritten as

follows [52]:

$$T = \frac{3}{4} P \frac{L_m}{L_r} i_{qs}^e \psi_{dr}^e \qquad (4.16)$$

Consequently, if the rotor flux, ψ_{dr}^e, is a constant value, the motor flux and

torque can be controlled independently based on a reference Torque, T^*, and a

reference flux, ψ_{dr}^{e*}, and equation (4.15) and (4.16) can be simplified further and

rewritten as following [52]:

$$i_{ds}^{e\,*} = \frac{\psi_{dr}^{e*}}{L_m} \qquad (4.17)$$

$$i_{qs}^{e\,*} = \frac{4T^* L_r}{3 L_m P \psi_{dr}^e} \qquad (4.18)$$

where, i_{ds}^{e*} and i_{qs}^{e*} are the stator reference current components in this reference

frame.

Hence, in a current controlled voltage-source inverter, the motor currents

should be controlled in real time to render these currents equal to the reference

current components, i_{ds}^{e*} and i_{qs}^{e*}, then one transfers these components, i_{ds}^{e*} and i_{qs}^{e*}, to

an a-b-c frame of reference to control the motor. Where, i_{ds}^{e*} and i_{qs}^{e*}, are

correspondingly calculated based on the commanded reference torque, T^*, and

reference d-axis flux, ψ_{dr}^{e*}. In the speed control mode, the reference torque is usually

obtained from an outer speed loop. Meanwhile, reference torque may be obtained

from an external reference in automated processes.

4.5 Analysis of the closed-loop motor-drive system including a fault mitigation controller under two-phase operation of a delta-connected induction motor

The fault mitigation strategy for the open-loop motor-drive system has been

introduced earlier in section 4.3 and it was extended here to the case of the closed-

loop vector control motor-drive system. The diagram of the closed-loop vector

control system including the fault mitigation controller is shown in Fig.4.5 [30]. In

this block diagram, the solid-line parts stand for the closed-loop motor-drive system

and dashed-line parts stand for the fault mitigation controller. For the closed-loop

vector controller, the speed and the flux were used as two reference signals, the speed

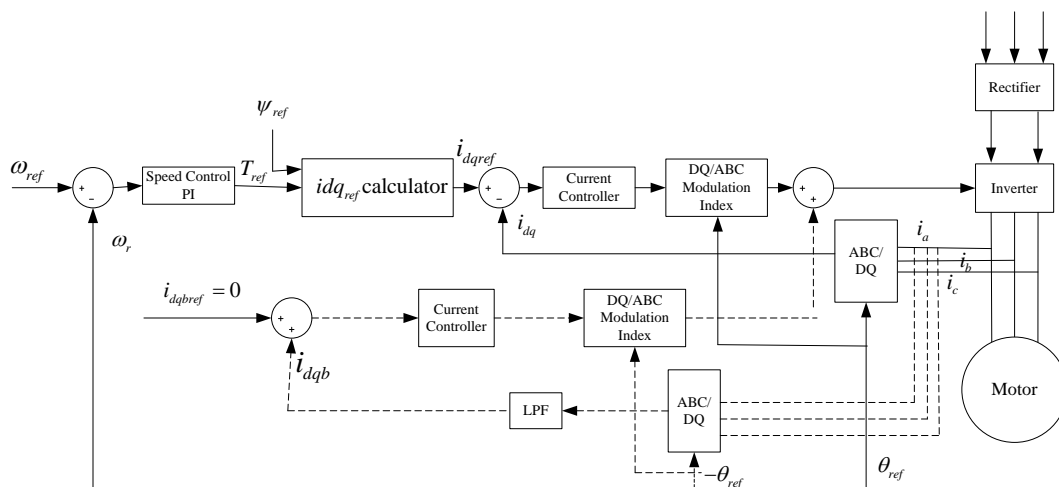and currents were measured and used as feedbacks.

Fig.4.5 Closed-loop vector control system including fault mitigation controller

The closed-loop vector control motor-drive system is more complex than the open-loop scalar control motor-drive system which has been introduced before. However, the fault mitigation controller for the closed-loop vector control motor-drive systems is somewhat similar to the open-loop scalar control motor-drive system. The theory of operation is still based on forcing the negative sequence current component to a value that is equal to, or at least close to, zero. This can be achieved through measuring the motor line currents and then transferring them from the a-b-c reference frame to a d-q-o reference frame rotating backward in a clockwise direction at a speed equal to the synchronous speed, utilizing an angle equal to but opposite to the rotor flux angle "θ_r". In the synchronous reference frame, the negative sequence current component appears as a dc value and the positive sequence current component appears as ac current ripple with a frequency equal to double the line frequency. The ac ripples in this frame can be filtered through a low pass (LPF). Then, the d-q dc current components are processed through the PI controllers to force these current components to a value equal to, or at least close to zero. The output of the PI controller is transferred back to the a-b-c reference frame and added to the main control signal, which is consequently processed to the modulator to generate the proper gating signal to the power switches of the drive system [30].

The simulink model of the controller is shown in Fig.4.6. The sampling frequency was also set to be 5K Hz. This was in order to readily compare the simulation results with the experimental results.
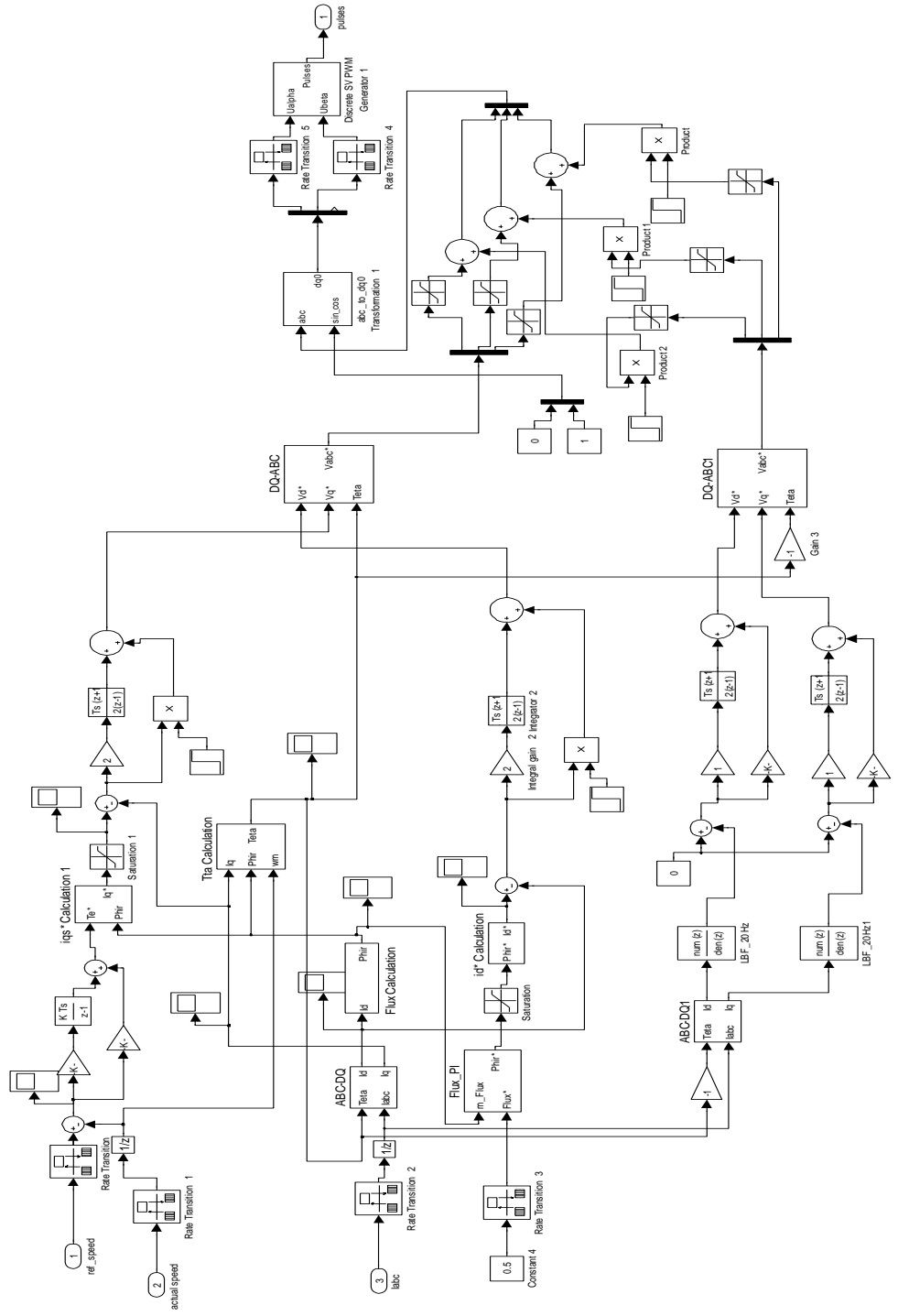
Fig.4.6 Simulink block diagram of the closed-loop vector control system including the fault mitigation controller

During the normal operation under the healthy three-phase case, the magnitude of the negative sequence current component is very small or nearly equal to zero. Hence, the magnitudes of the d-q current components in the previously mentioned counter-clockwise frame of reference are very close to, or at least nearly equals to zero. Therefore, the outputs of the two current PI controllers in the counter-clockwise current control loop are negligible and will have no effect on the modulator signal. On the other hand, the magnitude of the negative sequence current component will have a significant value under the two-phase open-delta mode of operation, in which one of the motor phases is isolated upon the detection of a phase winding's failure or due to an internal winding rupture in this phase. Hence, the magnitudes of the d-q current components in the synchronously rotating counter-clockwise frame of reference will have significant dc values. These dc values are processed through two PI controllers in the d-axis and q-axis. Therefore, the magnitudes of these current components can be forced to zero. The outputs of these two PI controllers are transformed back to the a-b-c reference frame which is added to the main modulator signal that correspondingly generate the proper gating signals that render a set of almost balanced motor line currents [30].

The entire closed-loop vector control motor-drive system including the fault mitigation controller linked to the MEC model implemented in the Matlab-Simulink environment is shown in Fig.4.7. Similar to the open-loop motor-drive system, the sampling time of the controller was set to be 200 micro-seconds and the sampling time of the MEC model and the inverter model was set to be two micro-seconds.

Hence a rate transition block was required between the MEC model and the controller,
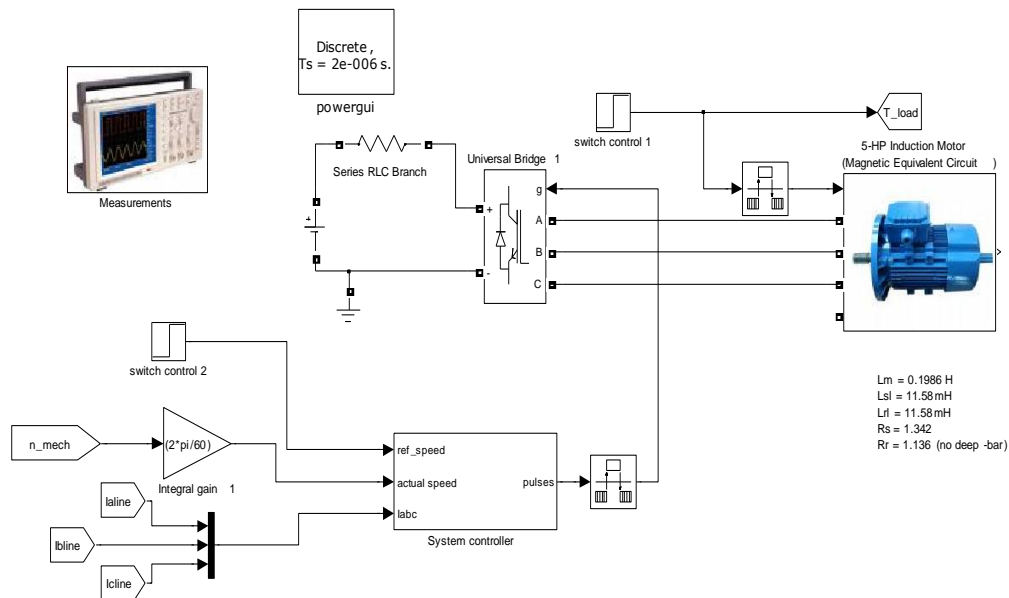
see Figure 4.7.

Fig.4.7 The entire closed-loop vector control motor-drive including the fault
mitigation controller implemented in Matlab-Simulink environment

Chapter 5
Simulation Results and Comparison to the TSFE Results and Experimental Test Data

5.1 Introduction

Both the open-loop scalar control motor-drive system, and the closed-loop vector control motor-drive system with the fault mitigation controller, have been introduced in the previous chapter. To verify the applicability and validity of this fault mitigation technique, and the accuracy of the MEC model discussed earlier, both the open-loop and the closed-loop motor-drive systems were simulated under several different operating conditions. The modes of operation can be mainly categorized into three cases. The first case was the normal healthy condition. In this case, the simulation results were obtained under the condition that the fault mitigation controller was activated. The main target of this category was to evaluate and verify the applicability, accuracy and the limitation of the MEC model used in the simulation with respect to the actual experimental setup. In addition, it also showed that the fault mitigation controller had no adverse effects on the performance of the delta-connected induction machine under the healthy three-phase operating condition. The second case was that of simulating the motor-drive system in the two-phase open-delta mode of operation with the fault mitigation controller disabled/deactivated. In this case, the simulation results were obtained under the condition that the fault mitigation controller was deactivated and the machine model was run under the two-phase open-delta faulty operating condition. The main purpose of this category was evaluating how the faulty operating condition can affect the performance of the

machine through observation of the line current waveforms and output torque profiles. The third case was simulating the motor-drive system in the two-phase open-delta mode of operation with the fault mitigation controller enabled/activated. The main target of this category was to show the performance of the fault mitigation controller simulated using the MEC machine model coupled to a PWM inverter under the faulty operating condition, which was the main focus of this thesis. The motor-drive system including the fault mitigation controller was linked to the MEC motor model and coupled to a PWM inverter. All the simulation was implemented in a Matlab-Simulink environment. In this chapter, all the simulation results obtained from the MEC model are shown, analyzed and compared to the results obtained from the TSFE model and the corresponding experimental setup [30]. The first objective was to verify the validity and applicability of the introduced fault mitigation technique. The second objective was to show the accuracy and fast-execution time of the MEC model. The MEC machine model can provide acceptable and accurate results with far less execution time compared to the TSFE simulation model of the same system.

5.2 Simulation results and comparison to the experimental results for the open-loop scalar control motor-drive system

In the open-loop scalar control motor-drive system, the sampling rate for the MEC model was one (1) micro-second. To make the results comparable with the experimental results, the sampling time for the controller was set to 200 micro-seconds which was the same sampling rate as the sampling rate of the DSP TMS320F2812 micro-processor. Accordingly, a rate transition was needed between the MEC model and the controller. Meanwhile, for the results obtained from the TSFE model, the sampling rate was set to 100 micro-seconds and the PWM inverter

was represented as a voltage source in this TSFE simulation model. The reference

frequency of the controller for both of these two models was 60 Hz.

5.2.1 The healthy condition operation with an enabled/activated fault mitigation
controller

The line currents obtained from the MEC model are shown in Fig. 5.1. There

is a set of balanced line currents with a peak value about 10 amperes. Meanwhile, the

line currents obtained from the TSFE model and the corresponding experimental

setup are shown in Fig. 5.2 and Fig. 5.3 [30]. These balanced line current waveforms

indicated that the effect of the activated fault mitigation controller on the motor-drive

system under the healthy operating condition was negligible, which was already

mentioned in Chapter 2 and was verified here. Meanwhile, the PWM inverter

switching effects on the line current waveform obtained from the MEC model can be

clearly distinguished from the line current waveforms obtained from the TSFE model.

The PWM inverter switching effects were naturally included in the experimental

results, which are given here in Fig. 5.3. The FFT spectra of the line current

waveforms obtained from the MEC model, from the TSFE model and the

corresponding experimental setup are shown in Fig.5.4 through Fig.5.6. The 60 Hz

fundamental frequency is clearly visible in all these three FFT spectra. The fifth,

seventh harmonics are also clearly visible in those FFT spectra of the motor line

currents.

The three motor phase current waveforms obtained from the MEC model,

from the TSFE model and the corresponding experimental setup [30] are shown in

Fig.5.7 through Fig.5.9. The amplitude of the phase currents in all three sets of results

is about 6 amperes. The PWM inverter switching effects on the phase current which

were fully included the phase current waveforms obtained from MEC model on the

current waveforms can also clearly be seen and distinguished from those waveforms

obtained from the TSFE model. The corresponding FFT spectra of the motor phase

currents obtained from MEC model, the TSFE model and the corresponding

experimental setup are shown in Fig.5.10 through Fig.5.12 [30]. One should notice

that the third, fifth and seventh harmonics are clearly visible in the FFT spectra of the

motor phase currents. These results show that the MEC model can provide reasonably

accurate results.
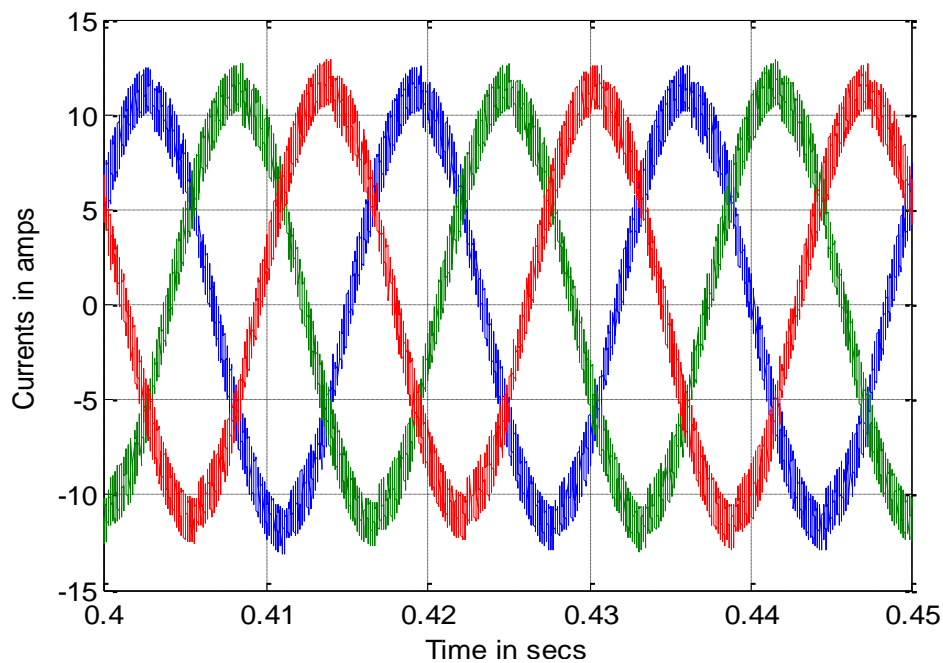
Fig.5.1 Three line currents, three-phase mode of operation, the fault mitigation
controller activated, MEC model
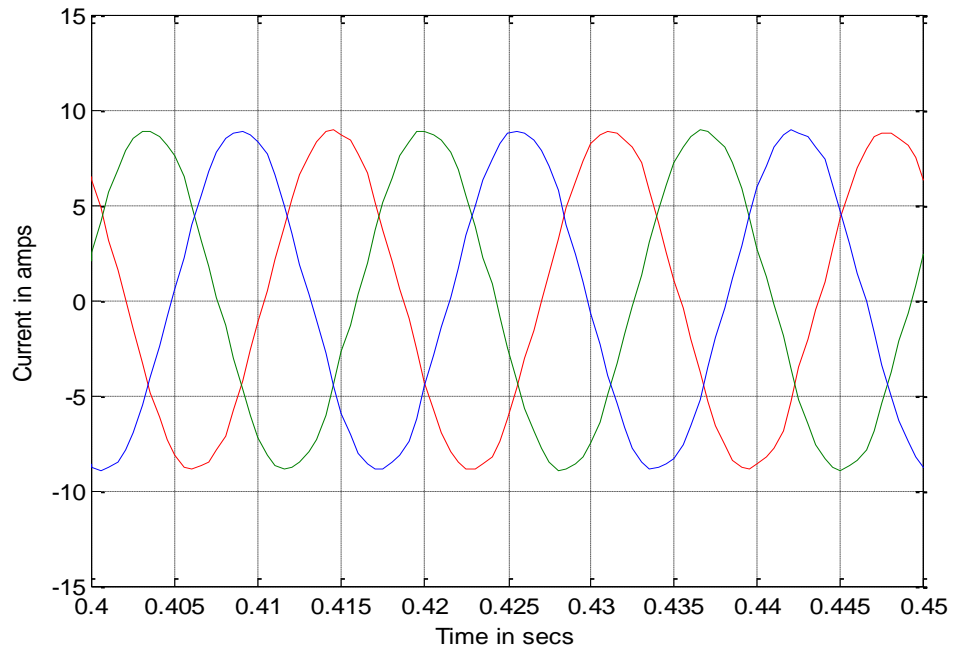
Fig.5.2 Three line currents, three-phase mode of operation, the fault mitigation controller activated, TSFE model
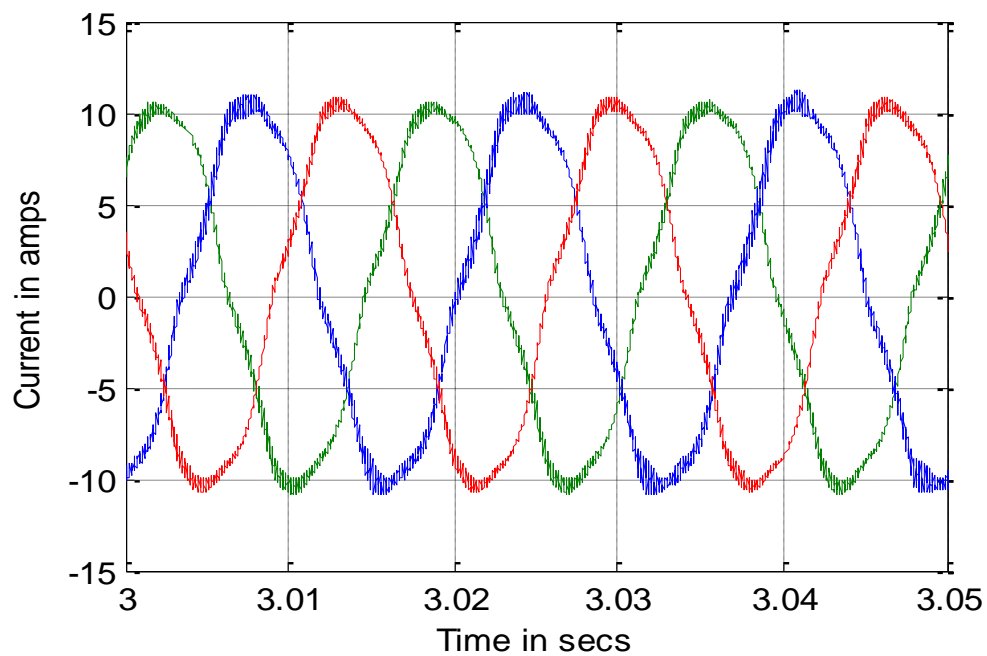
Fig.5.3 Experimentally obtained three line currents, three-phase mode of operation with the fault mitigation controller activated
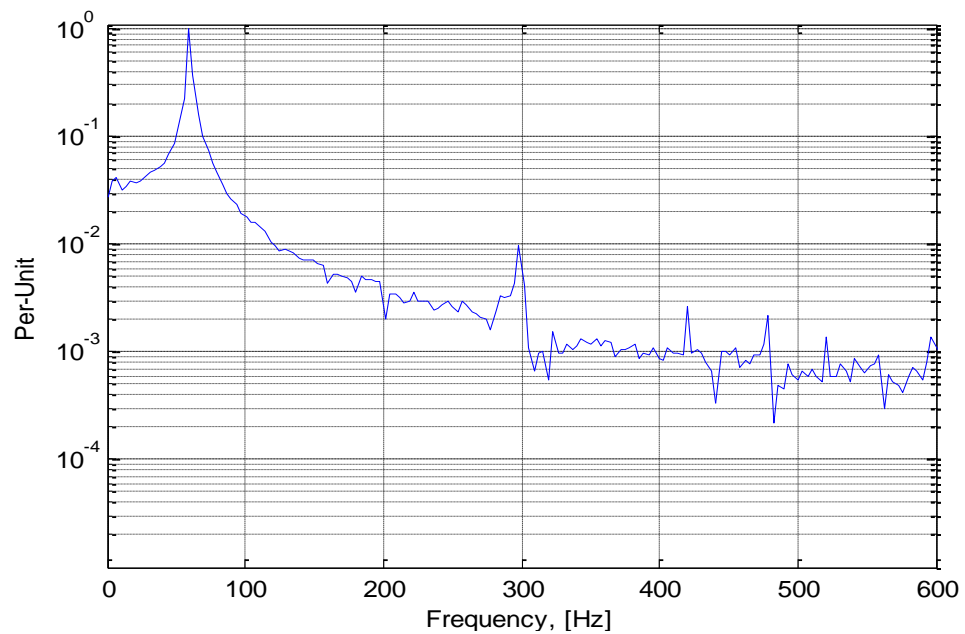
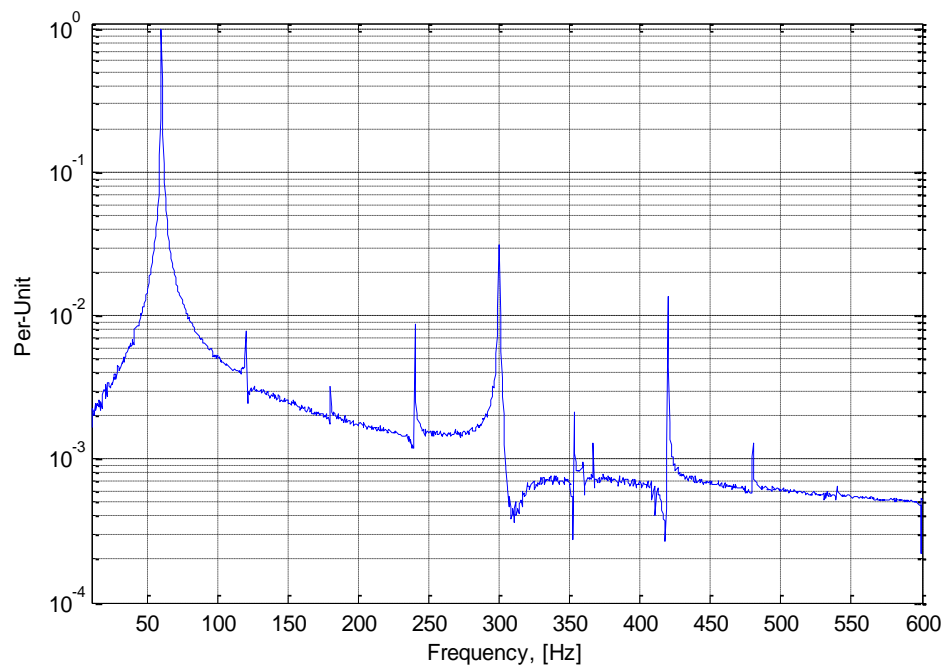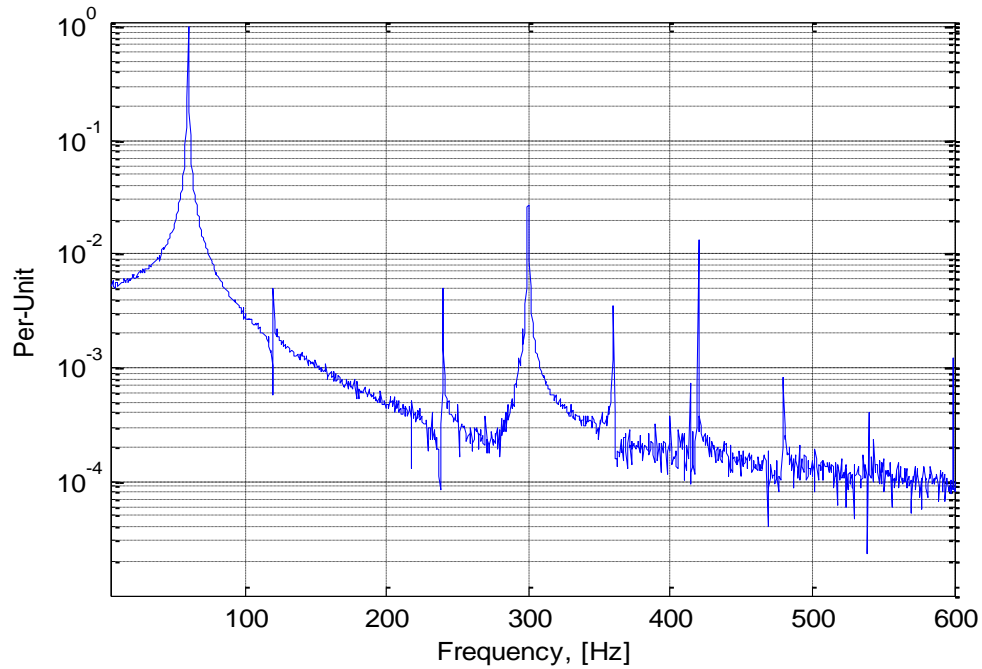Fig.5.4 Line current spectrum, three-phase mode of operation, the fault mitigation controller activated, MEC model

Fig.5.5 Line current spectrum, three-phase mode of operation, the fault mitigation controller activated, TSFE model

Fig.5.6 Experimentally obtained line current spectrum, three-phase mode of operation, the fault mitigation controller activated
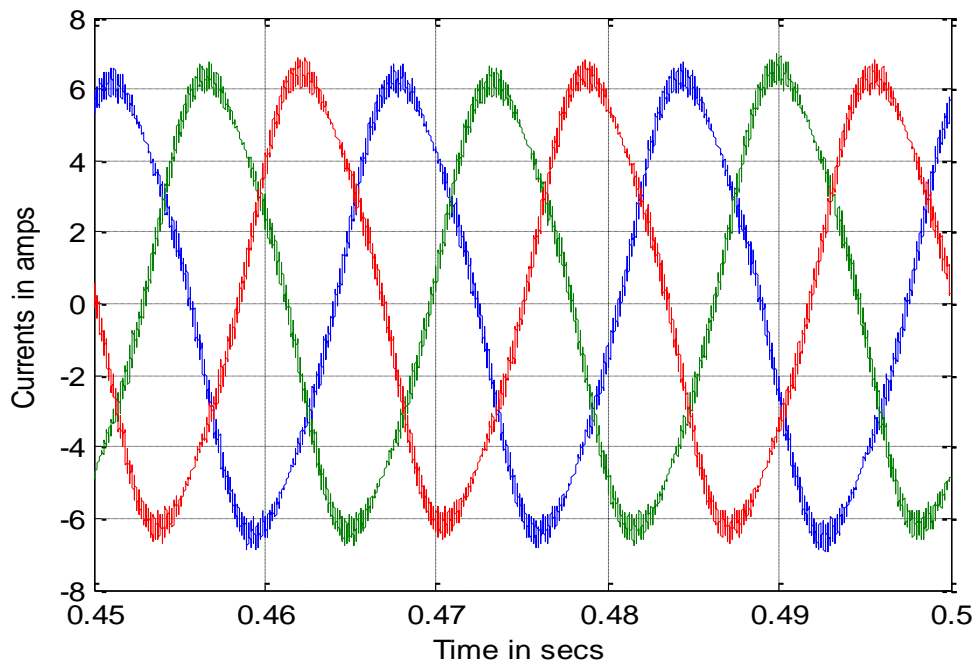

Fig.5.7 Three phase currents, three-phase mode of operation, the fault mitigation controller activated, MEC model
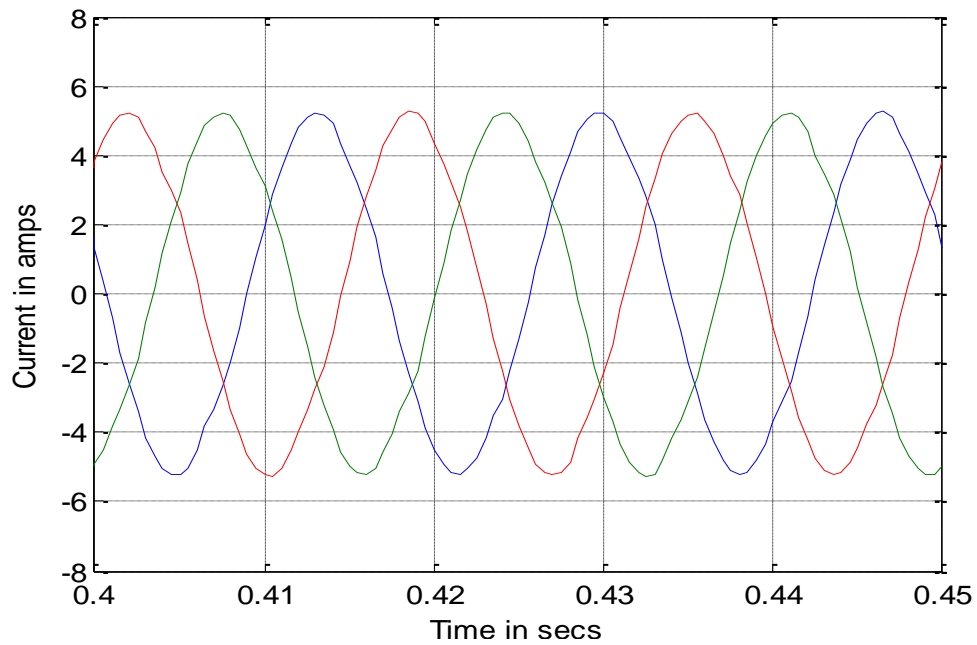
Fig.5.8 Three phase currents, three-phase mode of operation, the fault mitigation controller activated, TSFE model
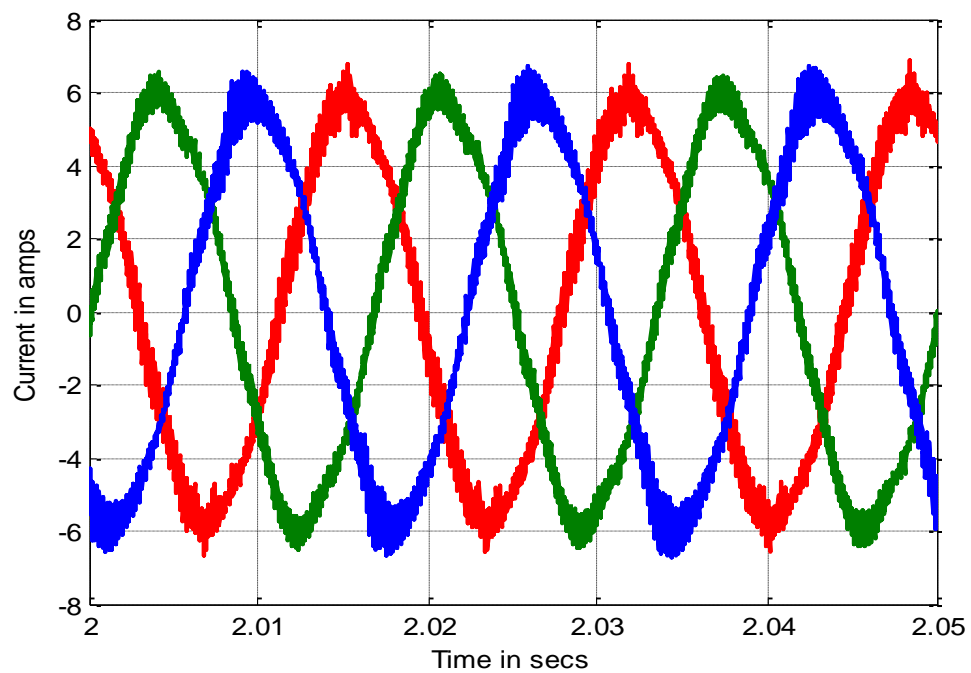

Fig.5.9 Experimentally obtained three phase currents, three-phase mode of operation with the fault mitigation controller activated
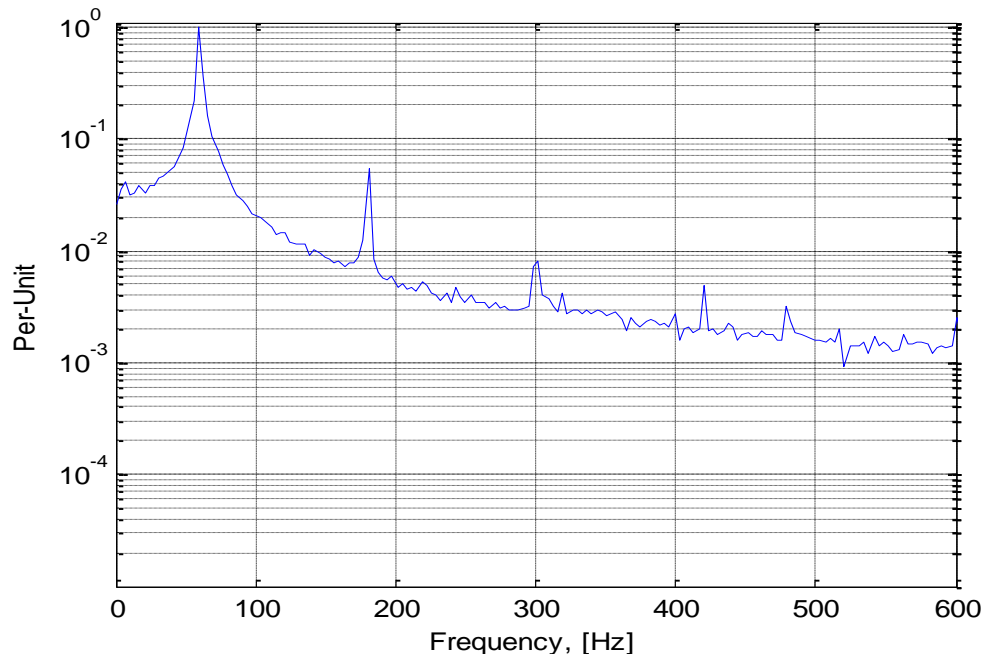
Fig.5.10 Phase current spectrum, three-phase mode of operation, the fault mitigation controller activated, MEC model
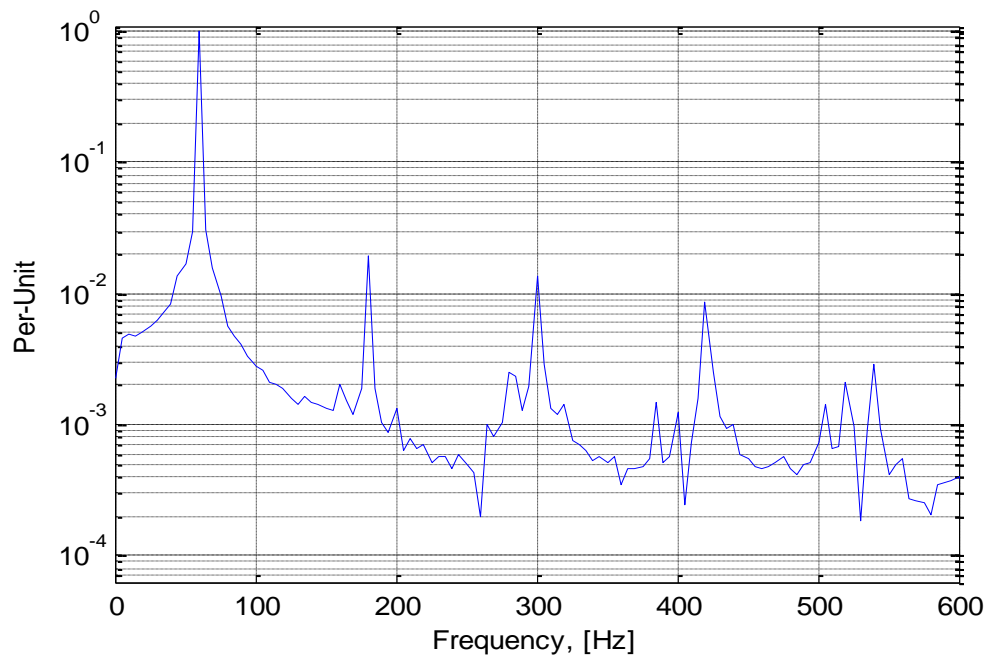

Fig.5.11 Phase current spectrum, three-phase mode of operation, the fault mitigation controller activated, TSFE model
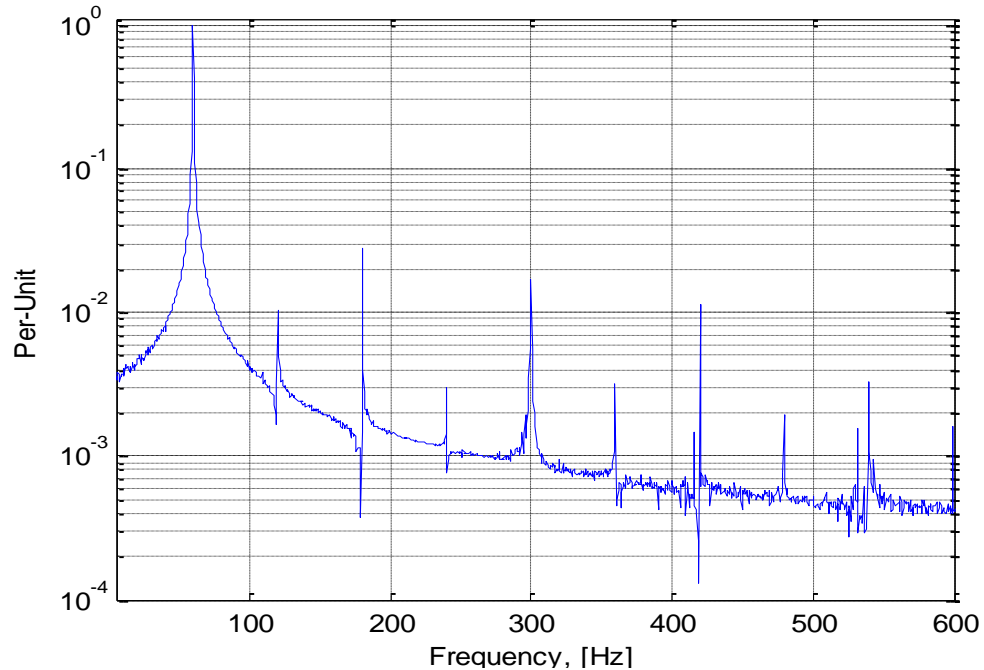
Fig.5.12 Experimentally obtained phase current spectrum, three-phase mode of
operation with the fault mitigation controller activated

5.2.2 The faulty condition operation with a disabled/deactivated fault mitigation
    controller

In this case, the model was simulated under the two-phase open-delta mode of

operation. The line current waveforms obtained from the MEC model are shown in

Fig.5.13. This is a set of three unbalanced line currents. The corresponding line

current waveforms obtained from the TSFE model and the experimental setup are

shown in Fig.5.14 and Fig.5.15 [30], respectively. This set of unbalanced machine

and drive line currents produced a backward rotating component of mmf, which could

cause excessive motor heating in the core and damper windings on the rotor, and

hence may cause damage to the machine and the drive system. In order to eliminate

the backward rotating mmf in the machine airgap and produce a set of balanced line

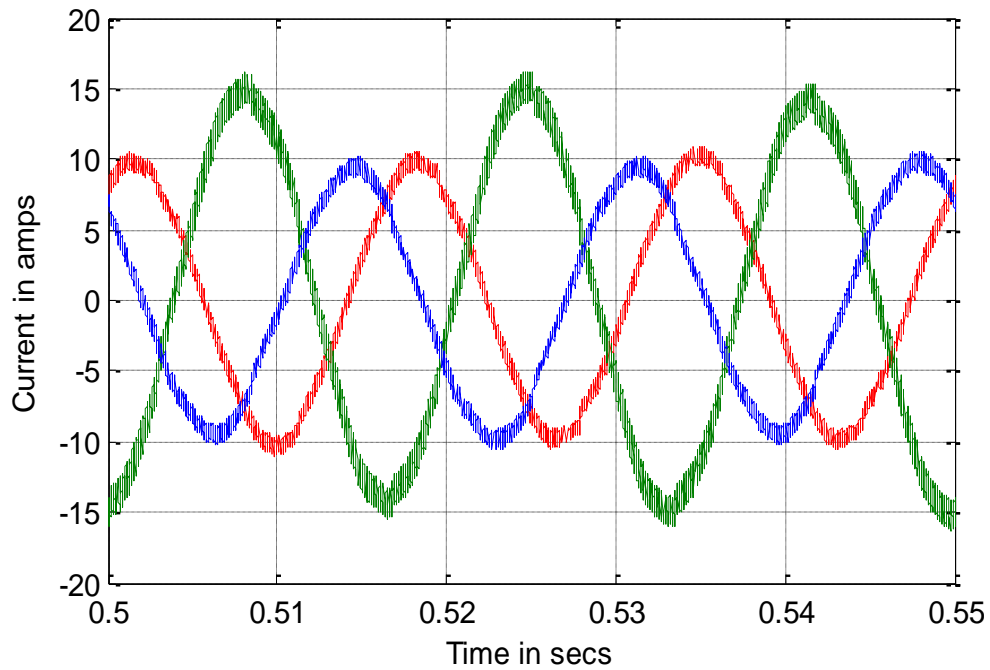currents, the fault mitigation controller needs to be enable/activated.

Fig.5.13 Three line currents, two-phase mode of operation, the fault mitigation controller deactivated, MEC model
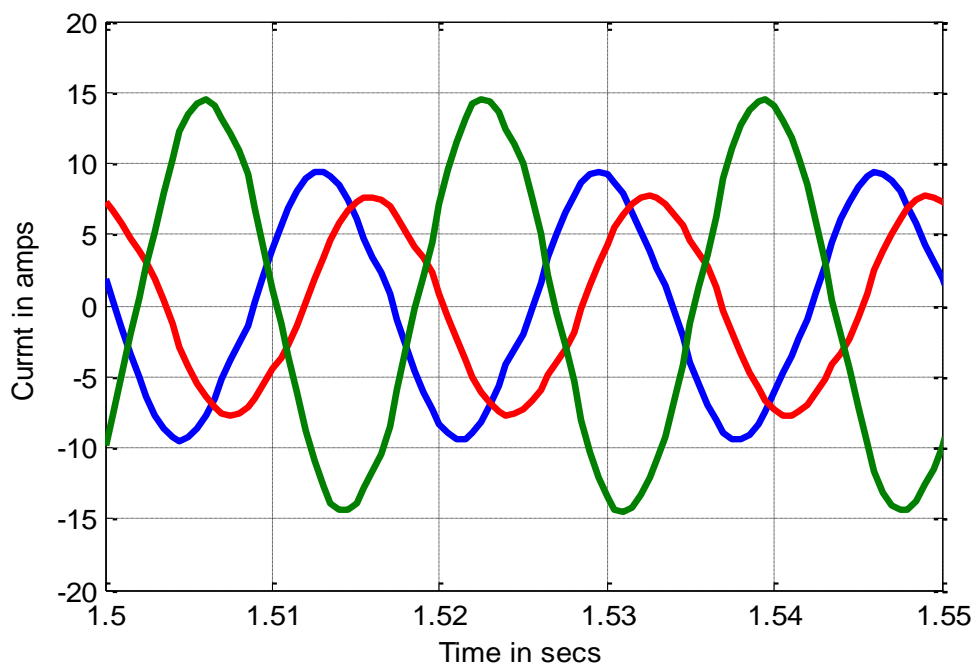

Fig.5.14 Three line currents, two-phase mode of operation, the fault mitigation controller deactivated, TSFE model
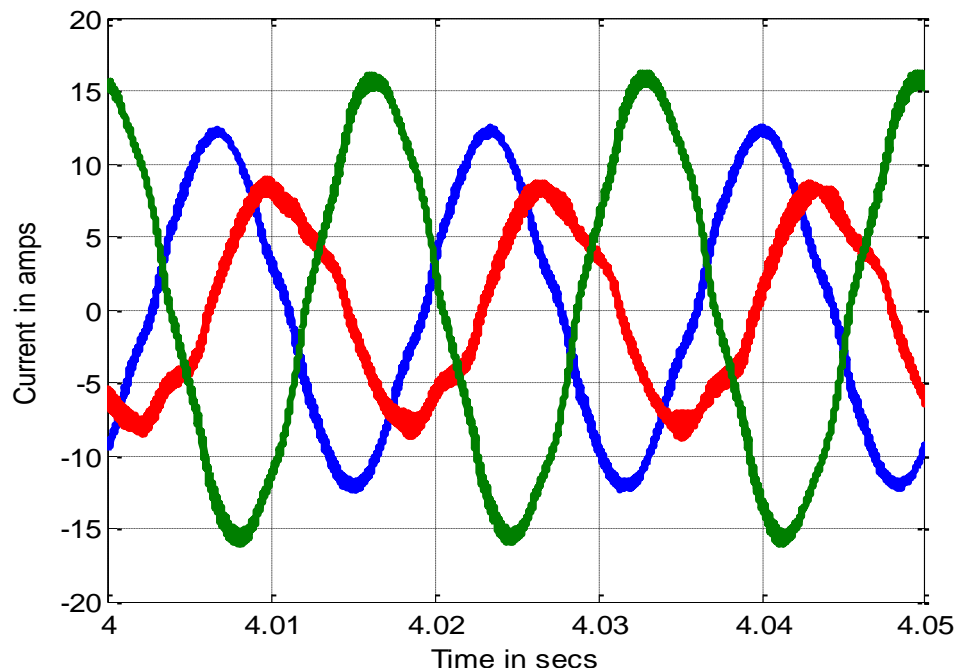
Fig.5.15 Experimentally obtained three line currents, two-phase mode of operation, the fault mitigation controller deactivated

5.2.3 The faulty condition operation with an enable/activated fault mitigation controller

The line current waveforms obtained from the MEC model, with the fault mitigation controller in an enabled/activated mode is shown in Fig.5.16. The corresponding line current waveforms obtained from the TSFE model and experimental setup, with the fault mitigation controller in an enabled/activated mode are shown in Fig.5.17 and Fig.5.18 [30], respectively. It can be clearly seen that with the fault mitigation controller in an activated mode, the motor-drive system can provide a set of almost balanced three-phase line currents, even when the machine is running under the two-phase open-delta mode of operation. The output torque profiles obtained from the MEC model, TSFE model and the corresponding experimental setup under the faulty operating condition with the fault mitigation controller in an

activated and a deactivated mode, are shown and compared in Fig.5.19 through

Fig.5.21 [30], respectively. These results show that with the fault mitigation

controller activated, the torque ripples can be reduced even under this faulty operating

condition. The three FFT spectra of the output torque profiles are shown in Fig.5.22

through Fig.5.24. The time harmonics in the line currents and the space harmonics in

the motor mmf waveforms had significant effects on the ripple contents of the output

torque when the machine was running under the two-phase open-delta operating

condition. As mentioned in Chapter 2, the machine may operate with a high torque

ripple of frequency equal to double the motor line current fundamental frequency, if a

fault happened while the machine was rotating. In addition, Sayed-Ahmed's previous

work [30] has already verified that the 120 Hz component was the main component of

the torque harmonics. It can be seen in Fig.5.22 through Fig.5.24 that the 120 Hz

torque components were reduced after enabling/activating the fault mitigation

controller. One should notice that in Fig.5.22, the FFT spectrum of the torque profile

obtained from the MEC model showed clearly that the 120 Hz component was 0.55 per

unit with a deactivated fault mitigation controller, and it decreased to a value of only

0.07 per unit after the fault mitigation controller was activated. In Fig.5.23, the FFT

spectrum of the torque profile obtained from the TSFE model showed that the 120 Hz

component was 0.64 per unit with a deactivated fault mitigation controller, while it

decreased to 0.062 per unit after the fault mitigation controller was activated. In

Fig.5.24, the FFT spectrum of the torque profile obtained from the corresponding

experimental setup showed that the 120 Hz component was 0.56 per unit with a

deactivated fault mitigation controller, while it decreased to 0.069 per unit after the
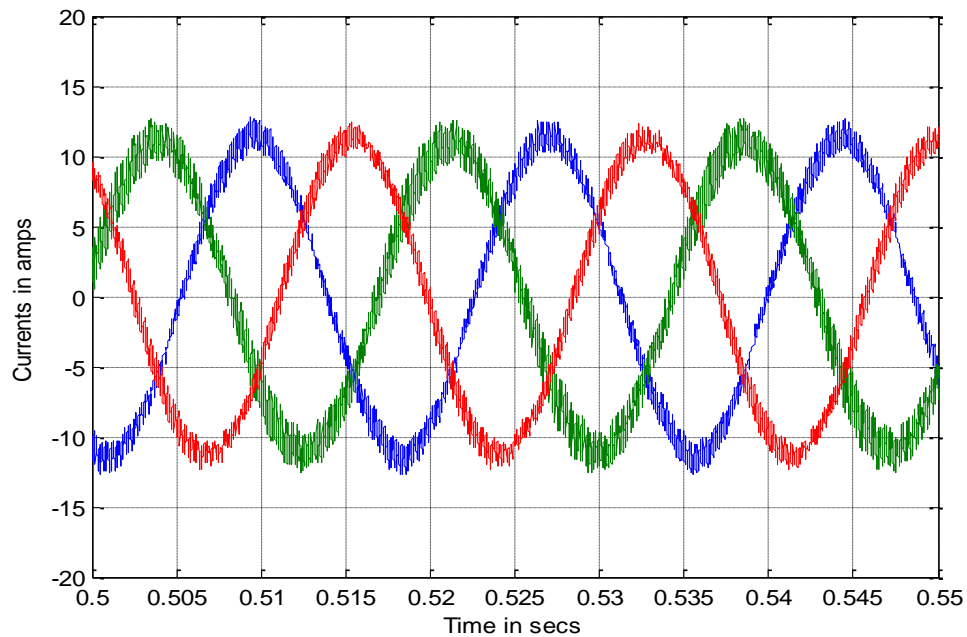
fault mitigation controller was activated.

Fig.5.16 Three line currents, two-phase mode of operation, the fault mitigation
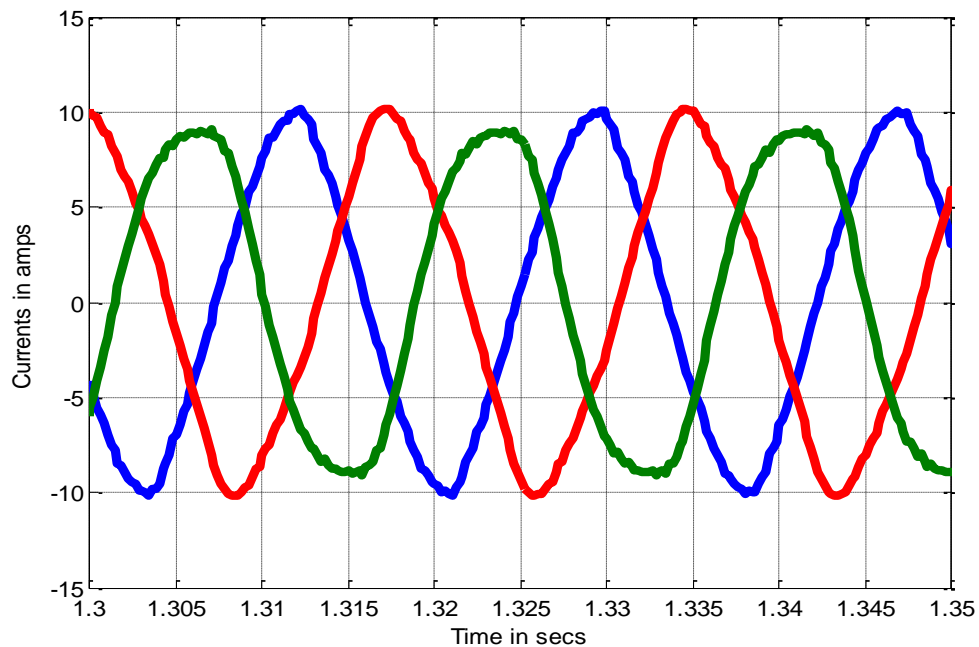controller activated, MEC model

Fig.5.17 Three line currents, two-phase mode of operation, the fault mitigation
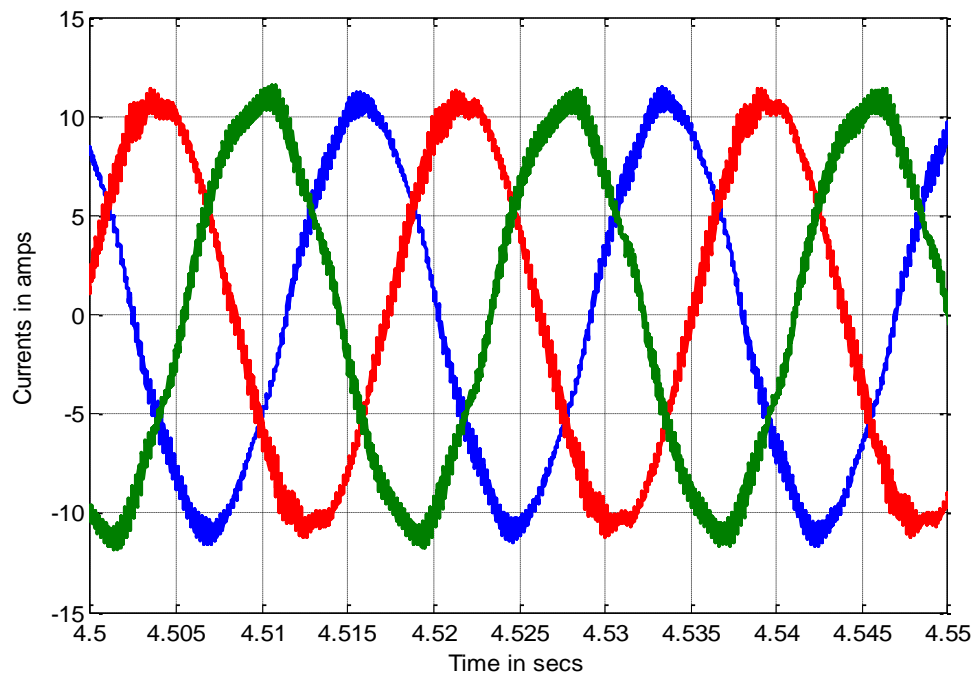controller activated, TSFE model

Fig.5.18 Experimentally obtained three line currents, two-phase mode of operation, the fault mitigation controller activated
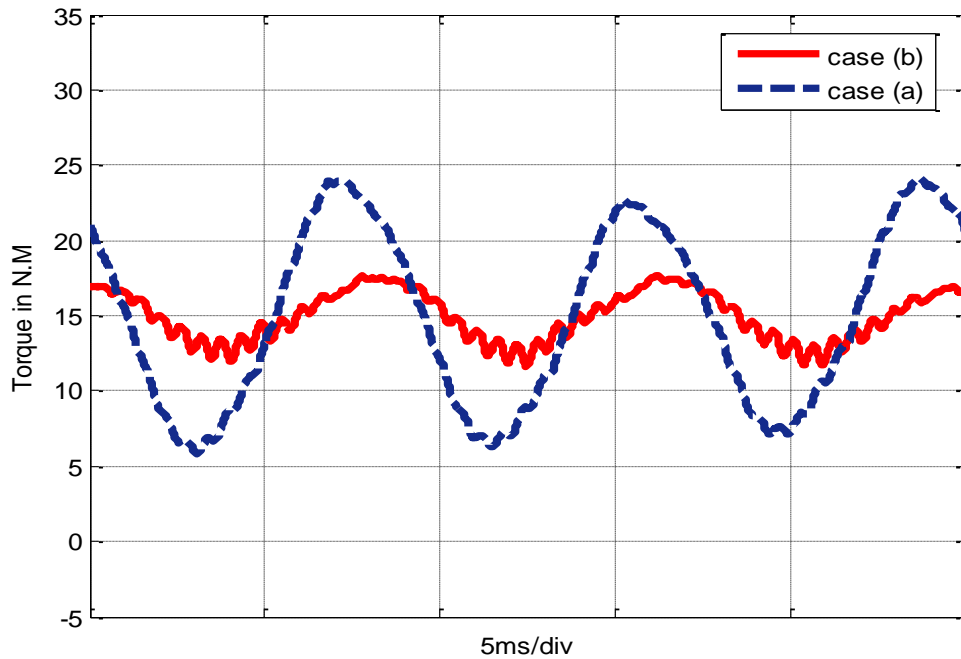

Fig.5.19 Output torque, two-phase mode of operation, MEC model: Case (a) the fault mitigation controller was deactivated, Case (b) the fault mitigation controller was activated
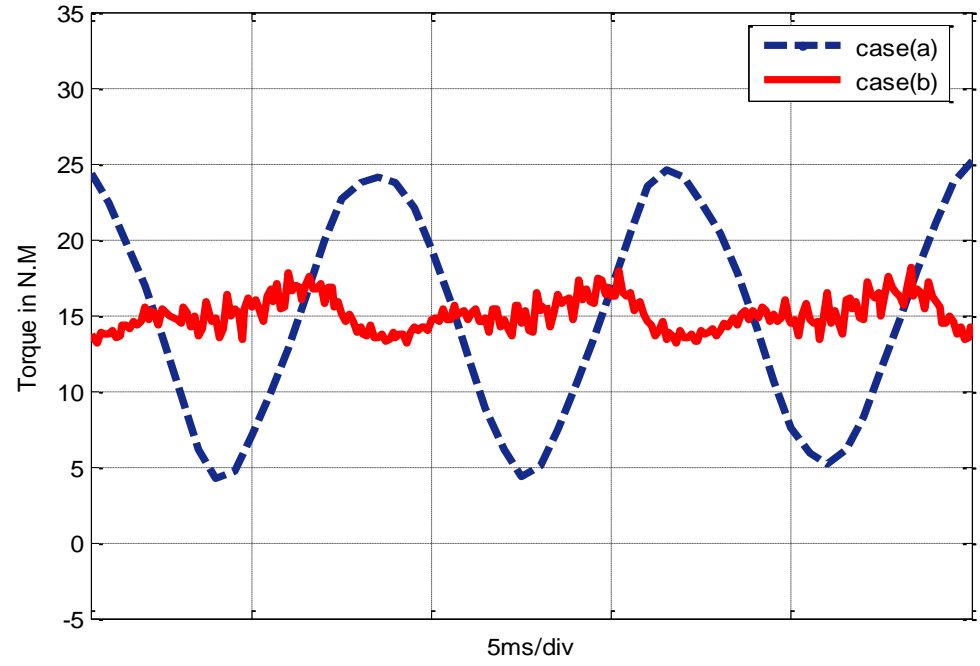
Fig.5.20 Output torque, two-phase mode of operation, TSFE model: Case (a) the fault mitigation controller was deactivated, Case (b) the fault mitigation controller was activated

Fig.5.21 Experimentally obtained output torque, two-phase mode of operation: Case (a) the fault mitigation controller was deactivated, Case (b) the fault mitigation controller was activated

Fig.5.22 Output torque spectrum, two-phase mode of operation, MEC model: Case (a) the fault mitigation controller was deactivated, Case (b) the fault mitigation controller was activated

Fig.5.23 Output torque spectrum, two-phase mode of operation, TSFE model: Case (a) the fault mitigation controller was deactivated, Case (b) the fault mitigation controller was activated
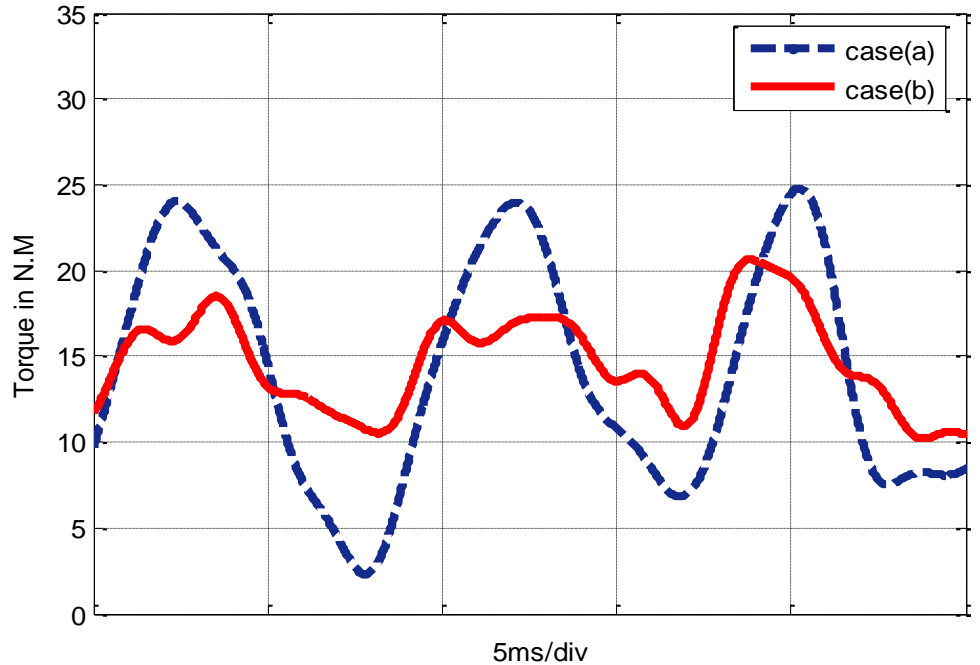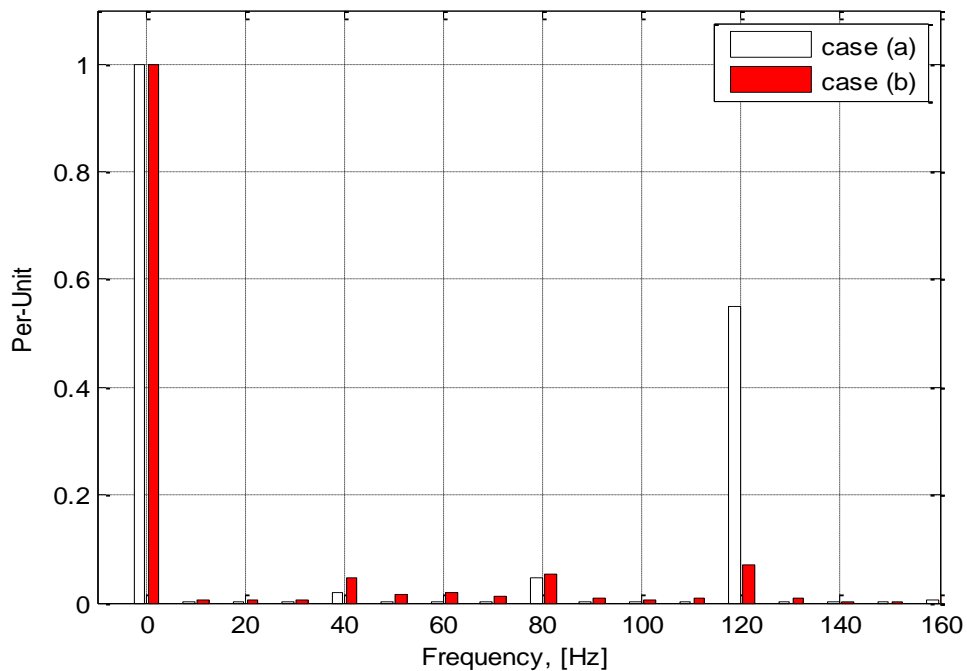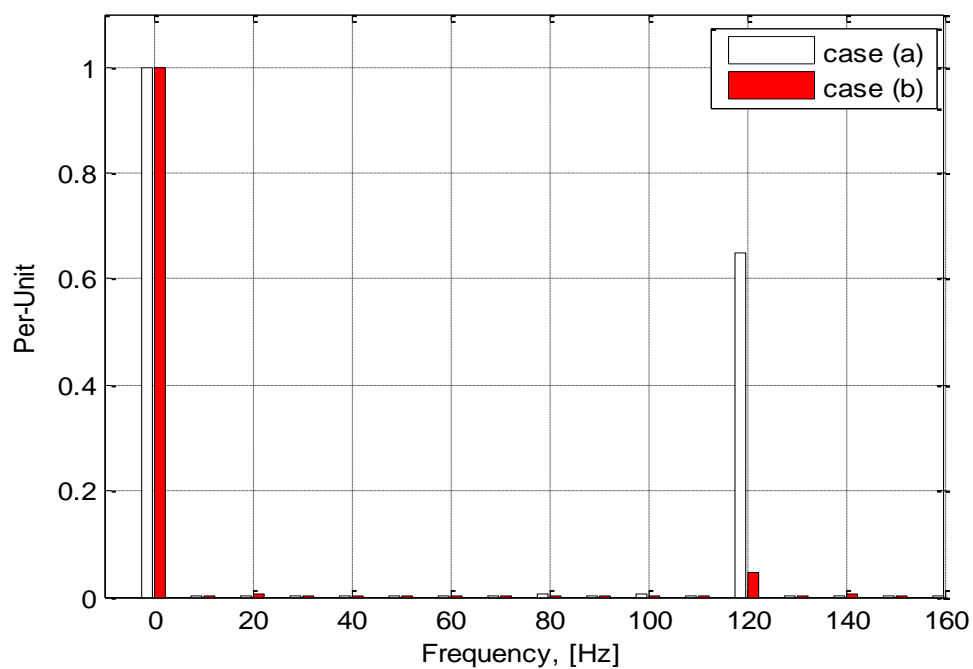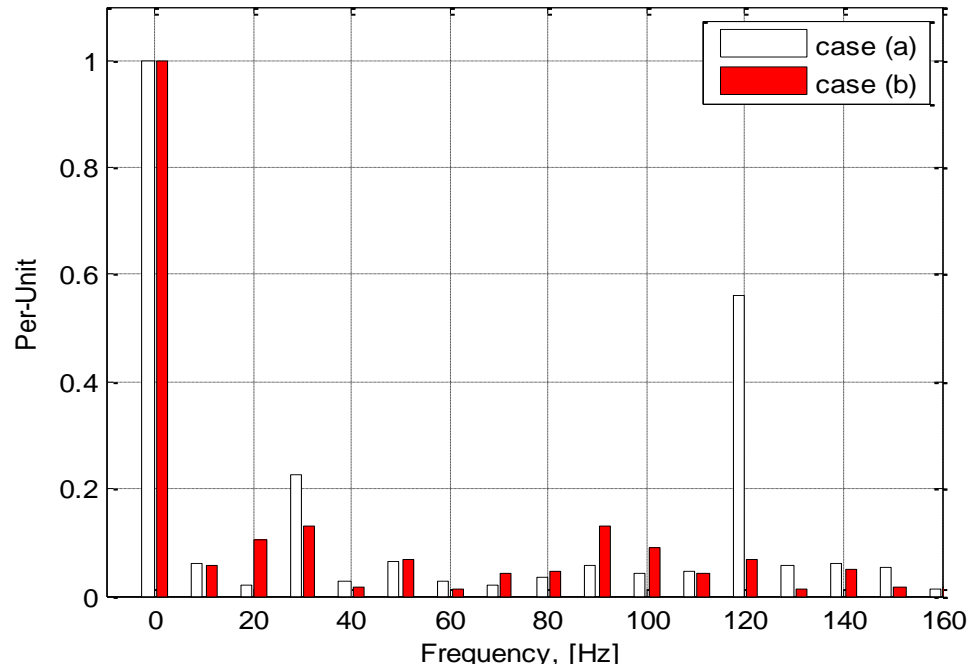
Fig.5.24 Experimentally obtained output torque spectrum: Case (a) the fault mitigation controller was deactivated, Case (b) the fault mitigation controller was activated

5.3 Simulation results and comparison to the experimental results for the closed-loop vector control motor-drive system

In the case of the closed-loop vector control motor-drive system, including the activation of the fault mitigation controller, the sampling rate for the MEC model and PWM inverter were two (2) micro-seconds. In the corresponding experimental setup, the introduced control algorithm was executed through an interrupt service routine called every 200 micro-seconds, and the carrier frequency was set to 5 kHz. To render the simulation results comparable with the experimental results [30], the sampling rate for the controller chosen to be 200 micro-seconds, which was the same as the sampling rate of the DSP TMS320F2812 micro-processor. Accordingly, a rate transition block was needed between the MEC model and the closed-loop motor-drive system including the fault mitigation controller. The reference angular frequency for

the controller was 120 rad./second. In a similar fashion to the open-loop motor-drive

system, the operation modes addressed in the closed-loop control system can be

divided into three main categories. The first category was the healthy operation mode,

when the introduced fault mitigation controller was activated. This was in order to

verify that the fault mitigation controller had no adverse effects on the system

performance under healthy operation. The second case was the faulty two-phase

open-delta mode of operation, when the fault mitigation controller was deactivated.

The main purpose of this category was to evaluate how the faulty operation condition

can affect the performance of the machine through observation of the line current

waveforms and output torque profiles. The third category was the faulty mode of

operation, when the fault mitigation controller was activated. The results in this

category showed the performance of the fault mitigation fault mitigation controller.

All the results obtained from the MEC model were compared to the results obtained

from the TSFE model and the corresponding experimental setup. Comparisons of

these results verified that the introduced fault mitigation controller improves the

performances of the delta-connected induction machine, even when the machine was

running under a two-phase open-delta faulty operating condition. In addition, the

MEC model coupled to a PWM inverter was shown here to provide acceptable and

reasonably accurate results with far less execution time.

5.3.1 The healthy condition operation with an enabled/activated fault mitigation controller

The three motor-drive line current waveforms obtained from the MEC model

and the TSFE model, under the healthy operating condition, at a reference speed

equal to 120 rad./second are depicted in Fig. 5.25 and Fig. 5.26, respectively. The

corresponding line current waveform obtained from the experimental setup is shown in Fig.5.27 [30].
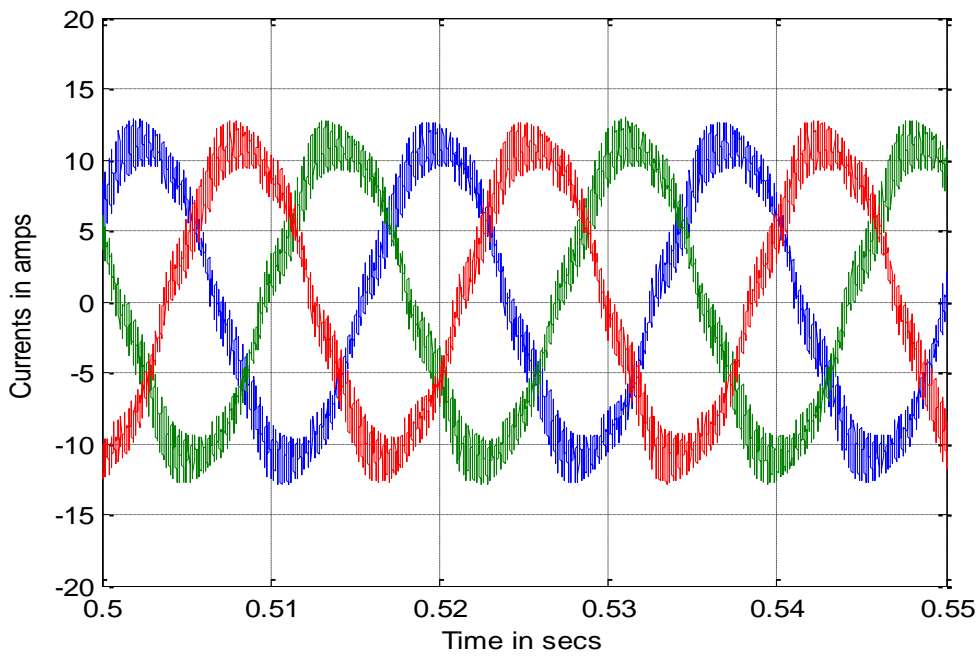

Fig 5.25 Three line currents, three-phase operation, compensation controller activated, MEC model
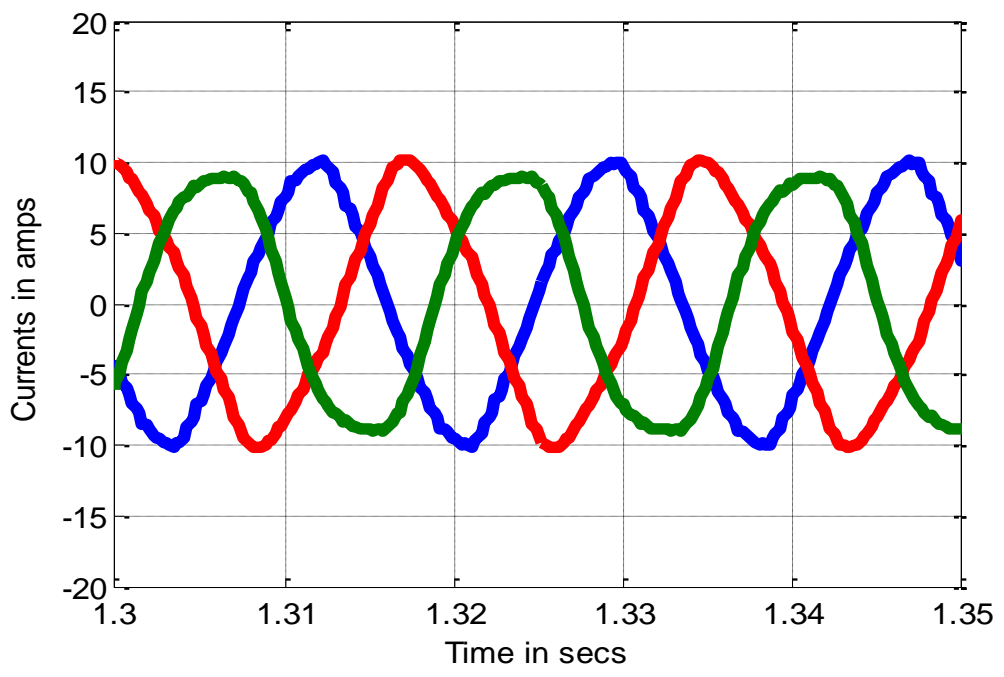

Fig. 5.26 Three line currents, three-phase mode of operation, the fault mitigation controller activated, TSFE model

Fig.5.27 Experimentally obtained three line currents, three-phase mode of operation
with the fault mitigation controller activated

5.3.2 The faulty condition operation with a disabled/ deactivated fault mitigation
     controller

In this case, the MEC model was simulated under the two-phase open-delta

mode of operation. The line current waveform obtained from the MEC model coupled

to a PWM inverter is shown in Fig.5.28. This is a set of three unbalanced line currents.

The corresponding line current waveforms obtained from the TSFE model and from

the experimental setup are shown in Fig.5.29 and Fig.5.30 [30], respectively. As

mentioned previously, this set of unbalanced motor-drive line currents produced a

backward rotating component of mmf waveform which could as explained earlier

damage the machine and the drive system. To eliminate this backward rotating mmf

in the closed-loop motor-drive system, the fault mitigation controller needs to be

enabled/activated.

Fig. 5.28 Three line currents, two-phase mode of operation, the fault mitigation
controller deactivated, MEC model

Fig.5.29 Three line currents, two-phase mode of operation, the fault mitigation
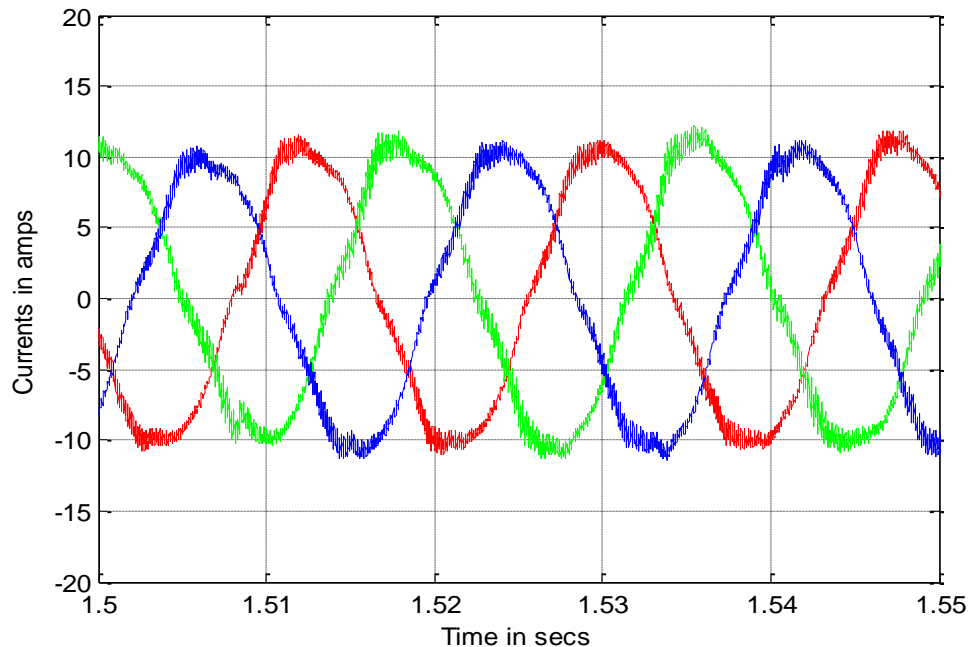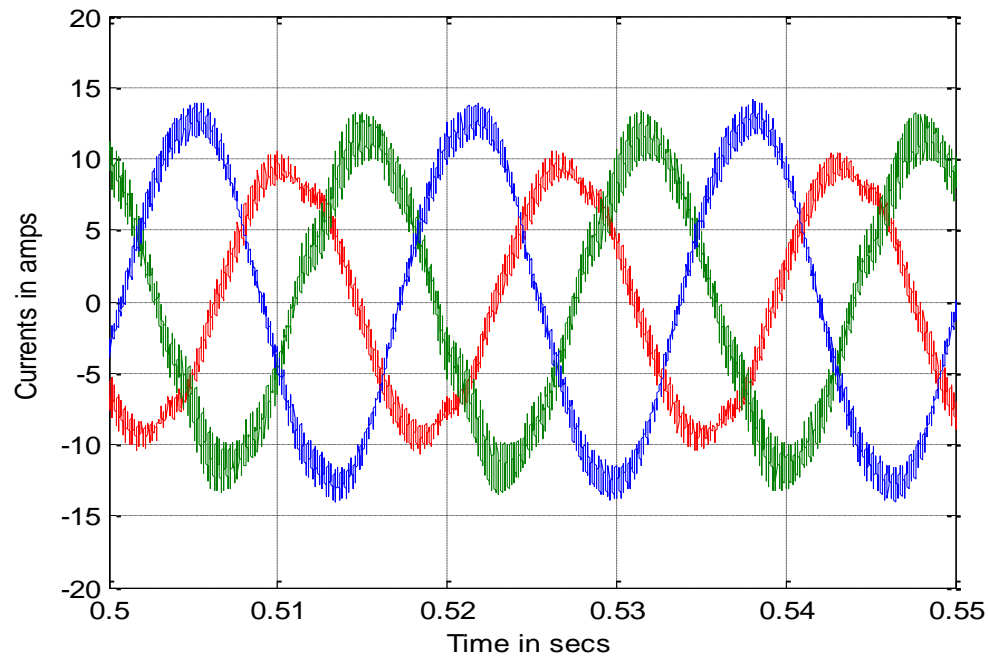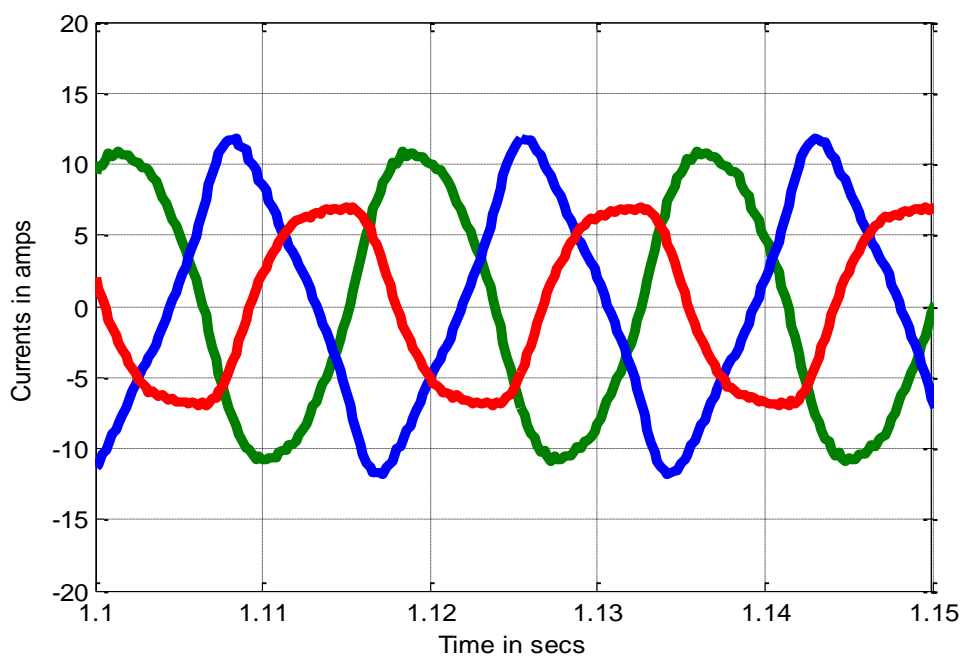controller deactivated, TSFE model

Fig.5.30 Experimentally obtained three line currents, two-phase mode of operation,
the fault mitigation controller deactivated

5.3.3 The faulty condition operation with an enabled/activated fault mitigation
    controller

In this case, the MEC model was simulated under the two-phase open-delta

mode of operation with the fault mitigation controller in an enabled/activated mode.

The line current waveforms obtained from the MEC model coupled to a PWM

inverter are shown in Fig.5.31. The corresponding line current waveforms obtained

from the TSFE model and from the experimental setup are shown in Fig.5.32 and

Fig.5.33 [30], respectively. It can be seen that the closed-loop motor-drive system

with an enabled/activated fault mitigation controller provides a set of almost balanced

line currents. The amplitude of this set of line currents was about 10 amperes. The

output torque profiles obtained from the MEC model, from the TSFE model and the

corresponding experimental setup under the two-phase open-delta faulty operating

condition with the fault mitigation controller activated and deactivated are shown and compared in Fig.5.34 through Fig.5.36 [30], respectively. These results show that with an enabled/activated fault mitigation controller, the output torque ripples were reduced significantly even when the machine was running under the two-phase open-delta faulty operating condition.
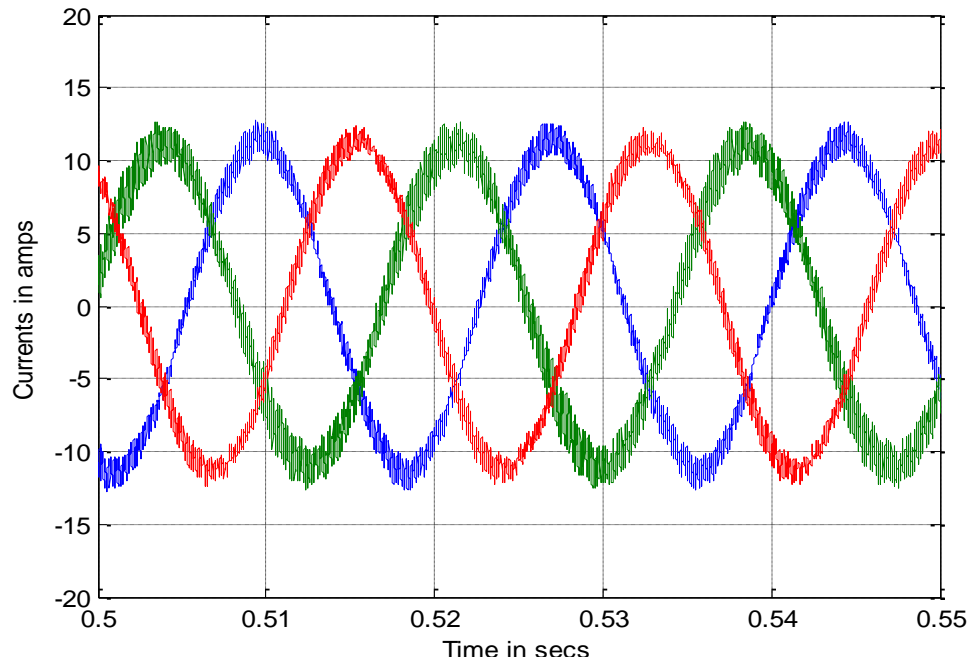
Fig.5.31 Three line currents, two-phase mode of operation, the fault mitigation controller activated, MEC model
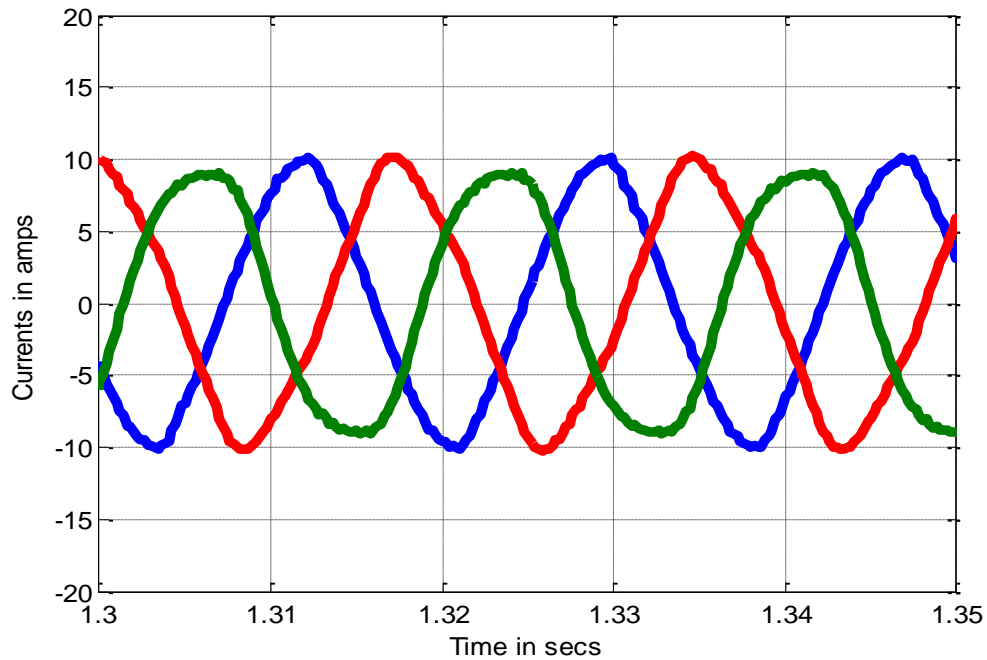
Fig.5.32 Three line currents, two-phase mode of operation, the fault mitigation
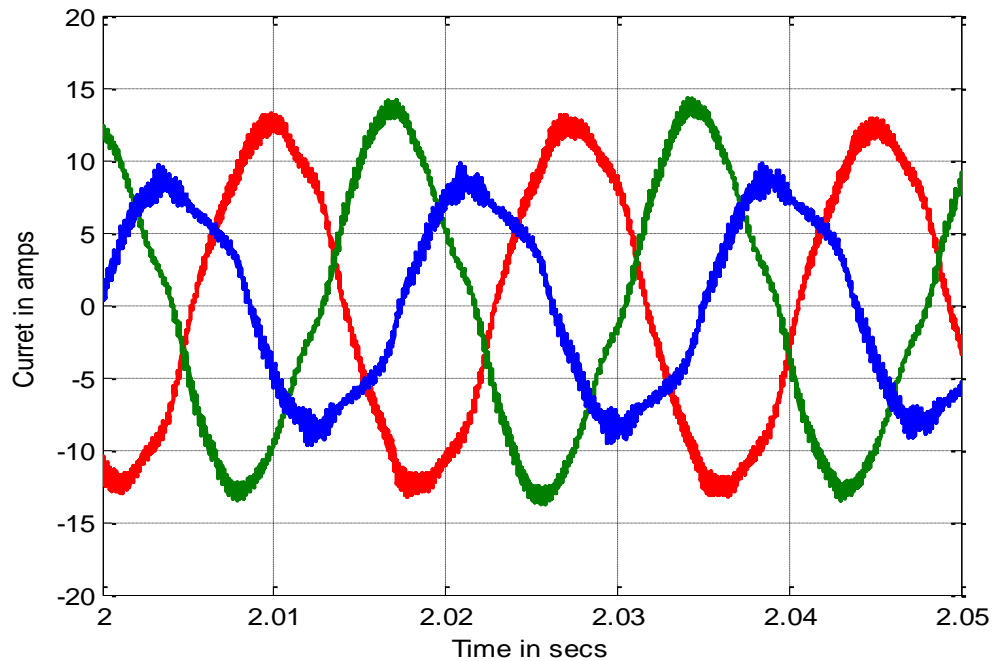controller activated, TSFE model
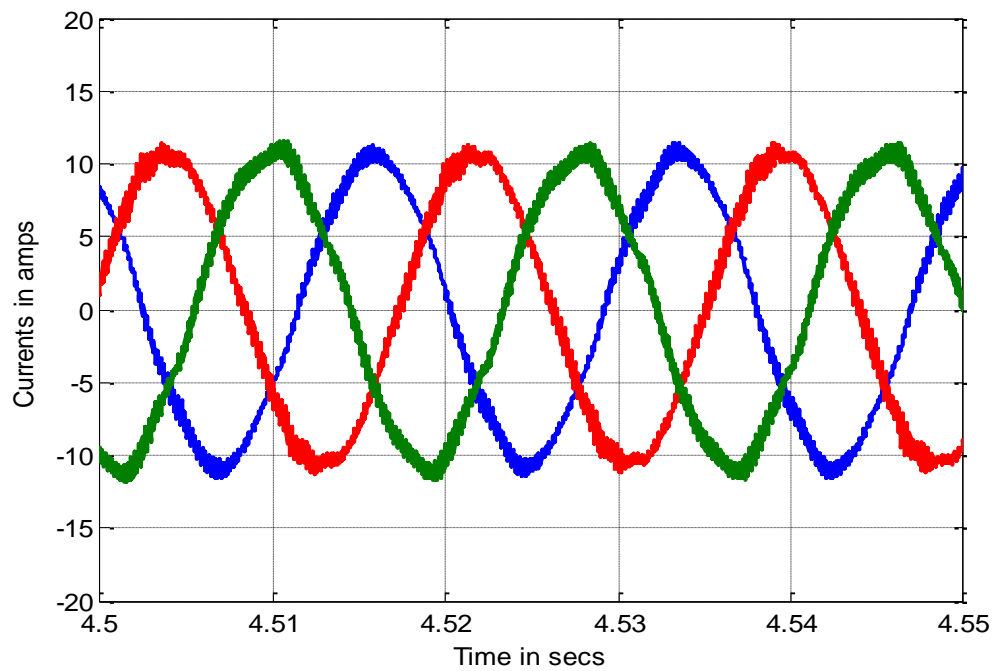
Fig. 5.33 Experimentally obtained three line currents, two-phase mode of operation,
the fault mitigation controller activated
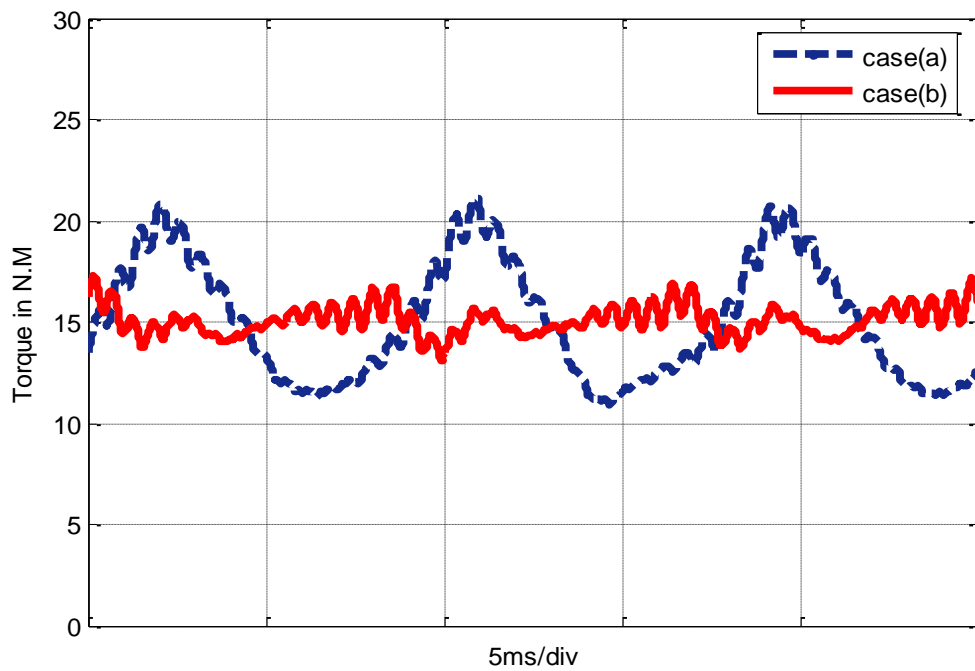
Fig.5.34 Output torque, two-phase mode of operation, MEC model. Case (a) the fault mitigation controller was deactivated. Case (b) the fault mitigation controller was activated
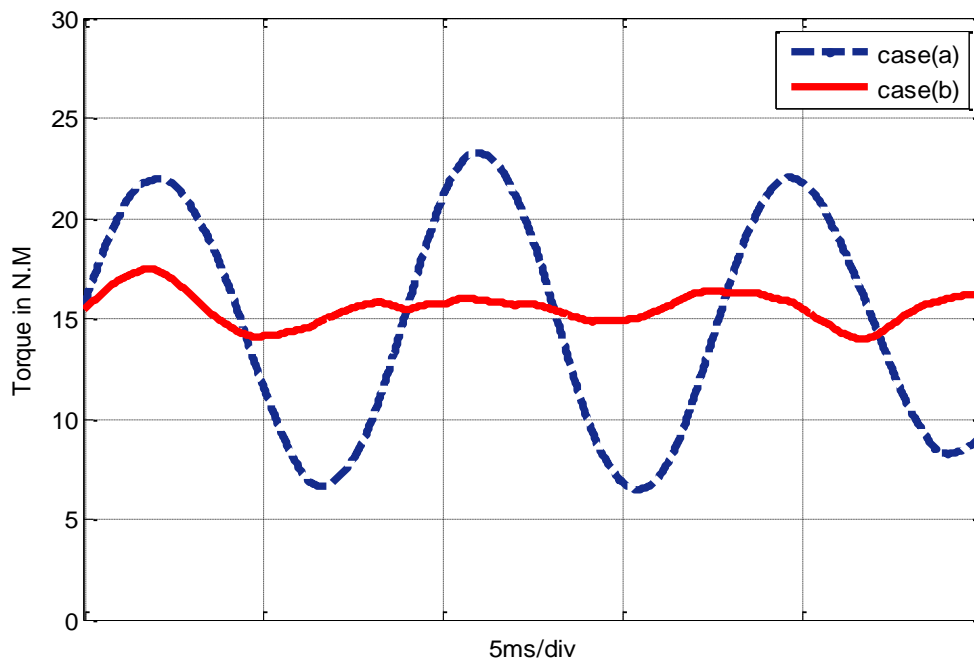
Fig.5.35 Output torque, two-phase mode of operation, TSFE model. Case (a) the fault mitigation controller was deactivated. Case (b) the fault mitigation controller was activated
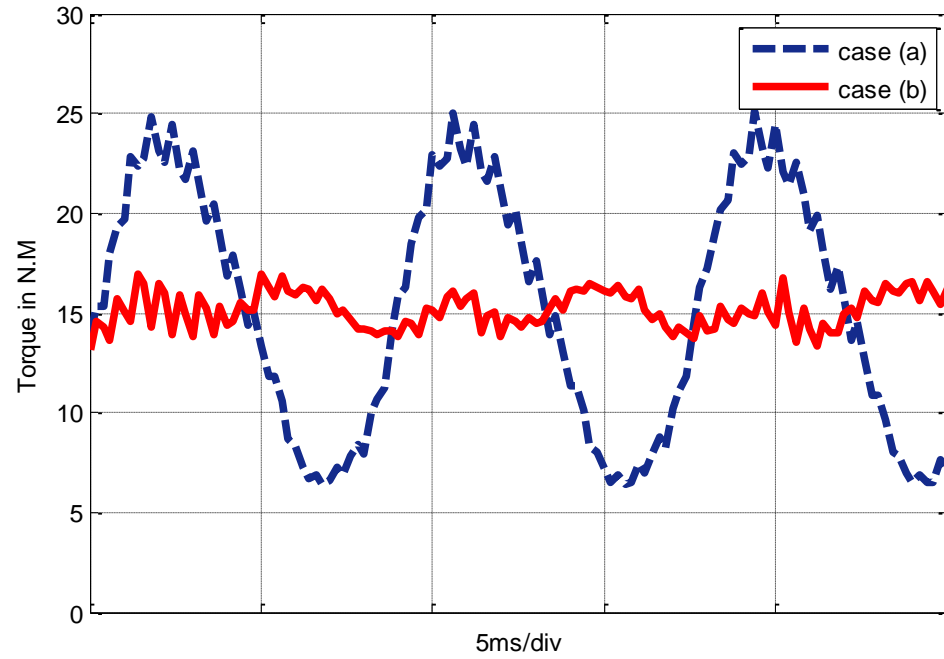
Fig.5.36 Experimentally obtained torque, two-phase mode of operation. Case (a) the fault mitigation controller was deactivated. Case (b) the fault mitigation controller was activated

Chapter 6
Conclusions and Future Work

6.1 Conclusions

In this thesis, a novel fault mitigation controller developed by Ahmed Sayed-Ahmed [30] was reviewed, and the Magnetic Equivalent Circuit (MEC) simulation models of both the open-loop scalar control and closed-loop vector control motor-drive systems including the fault mitigation controller were developed. The motor-drive systems were linked to the MEC model for a delta-connected induction machine, and its associated PWM inverter. The motor-drive system was simulated under both the healthy three-phase operating condition, and the two-phase open-delta faulty operating condition. The purpose of this thesis was to verify the applicability and validity of the fault mitigation algorithm and the accuracy of the MEC model in simulating such faults.

In Chapter 2, the modes of operation for both the healthy operating condition and two-phase open-delta faulty operating condition for a delta-connected induction machine were analyzed. Then the fault mitigation algorithm was explained utilizing the current space vector concept and point of view, and the stator resultant mmf point of view. It was shown that with an appropriate control algorithm, the fault mitigation controller can still generate a near perfect rotating mmf in the airgap and produce a set of almost balanced line currents even when the machine was running under the two-phase open-delta faulty operating condition.

In Chapter 3, the MEC modeling approach was introduced and a model for a 5-hp, delta-connected induction machine was given. The previous work already

showed that the MEC model can provide acceptable accurate results with far less execution time. This motor model was used in this thesis when linked to a PWM drive system including the fault mitigation controller, to verify the applicability and validity of this fault mitigation technique.

In Chapter 4, the basic principles of the open-loop scalar control motor-drive system and the closed-loop vector control motor-drive system including the fault mitigation controller were analyzed. Then the MEC motor model was coupled to a PWM inverter, thus linking the motor-drive systems including the fault mitigation controller. This global model was simulated under both the healthy three-phase operating condition and the two-phase open-delta faulty operating condition. The Matlab-Simulink block diagrams and the detailed simulation conditions were given.

In Chapter 5, all the simulation results obtained from the MEC model were given and compared to the results obtained from the TSFE model and the corresponding experimental setup. In order to analyze the applicability and validity of the fault mitigation algorithm, FFT spectra of the output torque profiles and current waveforms were given and analyzed. By comparing the current waveforms, torque profiles and FFT spectra, the applicability and validity of the fault mitigation technique and the accuracy of the MEC model were confirmed.

6.2 Future work

For future work, other fault mitigation methods for the motor-drive systems need to be investigated, implemented and verified using the MEC machine model and its associated drive system.

References

[1] N. Tesla, "Electro Magnetic Motor" U. S. Patent 381,968, May 1, 1888.

[2] N. Tesla, "Electro Magnetic Motor" U. S. Patent 382,279, May 1, 1888.

[3] P. F. Albrecht, J. C. Appiarius, and D. K. Sharma, "Assessment of the Reliability of Motors in Utility Applications-Updated," *IEEE Transactions on Energy Conversion*, Vol.1, pp. 39-46, December 1986.

[4] IEEE Committee Report, "Report of Large Motor Reliability Survey of Industrial and Commercial Installation, Part I and Part II," *IEEE Transactions on Industry Applications*, Vol. IA-21, pp. 853-872, July/August 1985.

[5] P. F. Albrecht, J. C. Appiarius, and D. K. Sharma, "Assessment of the Reliability of Motors in Utility Applications-Updated," *IEEE Transactions on Energy Conversion*, Vol.1, pp. 39-46, December 1986.

[6] M. L. Sin, W. L. Soong, and N. Ertugrul, "Induction Machine On-Line Condition Monitoring and Fault Diagnosis – A Survey," *Australian Universities Power Engineering Conference*, Chrischurch, New Zeland, 2003.

[7] IEEE Committee Report, "Report of large motor reliability survey of industrial and commercial installation, Part I and Part II," *IEEE Transactions on Industry Applications*, Vol.21, pp.853-872, July/August 1985

[8] R. Barron, Ed. *Engineering Condition Monitoring Practice, Methods, and Applications*. New York: Addison Wesley Longman Inc, 1996.

[9] "IEEE Guide for AC Motor Protection," IEEE std C37.96-2000, Sponsor: Power system relaying committee of the IEEE power engineering society

[10] G. Gentile, N. Rotondale, and M. Tursini "Investigation of inverter-fed induction motors under faulty conditions" Power Electronics Specialists conference, Vol.1, July 1992.

[11] Chih-Chieh Shen, Allen R. Hefner, David W. Berning, and Joseph B. Bernstein "Failure dynamics of the IGBT during turn-off for unclamped inductive loading Conditions," *IEEE Transactions on Industry Applications*, Vol.36, No.2, pp.614- 624,March/April 2000.

[12] R. S. Chokhawala, J. Catt, and L. Kiraly, "A discussion on IGBT short-circuit behavior and fault protection schemes" *IEEE Transactions on Industry Applications*, Vol. 31, No.2, pp. 256–263, March/April 1995.

[13] Gerhard Mitic, and Guy Lefranc "Localization of electrical-insulation and partial discharge failures of IGBT modules," *IEEE Transactions on Industry Applications*, Vol.38, No.6, pp.175-180, January/February 2005.

[14] N. A. O. Demerdash, "Design and Analysis of Electric Motors in Adjustable Speed Drives" class notes for EECE 185, Department of Electrical and Computer Engineering, Marquette University, Milwaukee, Wisconsin, Fall 2009.

[15] Debaprasad Kastha, and Bimal K. Bose "Investigation of fault modes of voltage fed inverter system for induction motor drive" *IEEE Transactions on Industry Applications*, Vol.30, No.4, pp.1028-1038, July/August 1994

[16] Michael L. Gasperi "Life prediction modeling of bus capacitors in AC variable frequency drives" *IEEE Transactions on Industry Applications*, Vol.41, No.6, pp.1430-1435, November/December 2005.

[17] R. S. Alwitt, and R.G. Hills "The chemistry of failure of aluminum electrolytic Capacitors," *IEEE Transactions on Parts, Materials and Packaging*, Vol.1, No.2, pp.28-34,September 1965.

[18] Hao Ma, and Linguo Wang "Fault diagnosis and failure prediction of aluminum

electrolytic capacitors in power electronic converters" Industrial Electronics Society, IECON 2005. 31st Annual Conference of IEEE, pp. 6-10.

[19] Afroz M. Imam, "Condition monitoring of electrolytic capacitors for power electronics applications" Ph.D dissertation, Georgia Institute of Technology, May 2007.

[20] Sam G. Parler "Selecting and applying aluminum electrolytic capacitors for inverter applications" White paper, http://www.cde.com

[21] Jiri Klima, "Analytical investigation of influence of dc-link voltage ripple on PWM VSI fed induction motor drive", IEEE ICIEA 2006

[22] A Literature Review of IGBT Fault Diagnositc and Protection Methods for Power Inverters," *IEEE Transactions on Industry Applications*, pp 1770-1777, Septerber/October 2009

[23] G.Mahmoud, M.Masoud, I.EI-Arabawy "Rectifier Fault in Variable Voltage Variable Frequency Induction Motor Drives" Electric Machines and Drives Conference, 2007.

[24] J.A.A.Caseiro, A.M.S.Menders, A.J.Marques Cardoso "Fault Diagnosis on PWM Rectifier AC Drive System with Fault Tolerance Using the Average Current Park's Vector Approach", Electric Machines and Drives Conference, 2009.

[25] T.Jahns "Improved reliability in solid-state drives for large asynchronous ac machines by means of multiple-independent phase-drive units" Ph.D thesis, MIT, Cambridge,April 1978.

[26] T.Jahns "Improved reliability in solid-state drives for large asynchronous ac machines by means of multiple-independent phase-drive units," *IEEE Transaction on Industry Applications*,Vol.1A-16, No.3, pp 321-331, May/June 1980.

[27] R.L.A.Ribeiro, C.B.Jacobina,E.R.C da Silva, and A. M. N. Lima "A fault tolerant motor-drive system by using a compensated strategy on the PWM-VSI topology" IEEE Power Electronics Specialists Conference, 2001,pp.1191- 1196.

[28] Sebastio E.M de Oliveira "Operation of three-phase induction motors connected to one phase supply," *IEEE Transcations on Energy Conversion*, Vol.5, No.4, pp.713-718, December 1990

[29] Sepe R.B.Jr., B. Fahimi, C. Morrison Miller, M. John, "Fault Tolerant Operation of Induction Motor Drives with Automatic Controller Reconfiguration", Electrical Machines and Drives, 2001, pp.156-162.

[30] Ahmed Sayed Ahmed, "Control of PWM AC Motor-drive Systems under Faulty Conditions" Ph.D. dissertation, Marquette University, Milwaukee, Wisconsin, USA, August 2009.

[31] N.Erturgi, W.soong, G.Dostal, and D.Saxon "Fault tolerant motor drive system with redundancy for critical applications," Power Electronics Specialists Conference 2002, Vol.3, pp.1457-1462.

[32] Brian A. Welchko, Thomas A. Lipo, Thomas M. Jahns, and Steven E. Schulz "Fault tolerant three-phase AC motor drive topologies: A comparison of features, cost, and limitations," *IEEE Transactions on Power Electronics*, Vol.19, No.4, pp.1108-1116, July 2004.

[33] Youngkook, and Habetler "A stator turn fault tolerance strategy for induction motor drives in safety critical applications" Power Electronics Specialists Conference, 2006, PESC'06, 37th IEEE.

[34] R.S. Miranda, H.A.Toliyat, C.B.Jacobina, and A.M.N. lima "Short-circuit fault mitigation in six-phase induction machine drives" IEEE Vehicle Power and Propulsion Conference 2007, pp.370-376.

[35] S. D. Sudhoff, B. T. Kuhn, K. A. Corzine, and B. T. Branecky, "Magnetic Equivalent Circuit Modeling of Induction Motors," *IEEE Transactions on Energy Conversion*, Vol. 22, No. 2, pp.259-270, June 2007.

[36] Vlado Ostovic, "A Simplified Approach to Magnetic Equivalent Circuit Modeling of Induction Machines," *IEEE Transactions on Industrial Applications*, VOL 24, No.2, pp 308-316, Match/April, 1988.

[37] Homayoun Meshgin-Kelk, Jafar Milimonfared, and Hamid A. Toliyat, "Interbar Currents and Axial Fluxes in Healthy and Faulty Induction Motors," *IEEE Transactions on Industrial Application*, VOL 40, No.1, p 128-134, January/February, 2004.

[38] Gennadi.Y.Sizov, "Analysis, Modeling, and Diagnostic of Adjacent and Nonadjacent Broken Rotor Bars in Squirrel-Cage Induction Machines" M.S Thesis, Marquette University, Milwaukee, Wisconsin, USA, December 2007.

[39] Gennadi.Y.Sizov,Chia-Chou Yeh , N. A. O. Demerdash, " Magnetic equivalent circuit modeling of induction machines under stator and rotor fault conditions," Electric Machines and Drives Conference, 2009.

[40] A. E. Fitzgerald, C. Kingsley, S. D. Umans, *Electric Machinery*. 6th Edition, New York, McGraw-Hill, 2003.

[41] P.Vas, *Electrical machines and drives: a space-vector theory approach*. Oxford university press, 1992.

[42] M. L. Barnes and C. A. Gross, "Comparison of Induction Machine Equivalent Circuit Models, *System Theory, 1995, Proceedings of the Twenty-Seventh Southeastern Symposium on*, pp.14-17, March 1995.

[43] N. A. O. Demerdash, "Advanced Concepts in Analysis and Design of Electric Machines and Drives" class notes for EECE 285, Department of Electrical and Computer Engineering, Marquette University, Milwaukee, Wisconsin, Spring 2010.

[44] X. Luo, Y. Liao, H. A. Toliyat, A. El-Antably, and T. A. Lipo, "Multiple Coupled Circuit Modeling of Induction Machines," *IEEE Transactions on Industry Applications*, Vol. 31, No. 2, pp.203-210, March/April 1995.

[45] N. A. O. Demerdash, "Computer-Aided Field Calculations in Electrical Engineering Using Finite Elements" class notes for EECE 281, Department of Electrical and Computer Engineering, Marquette University, Milwaukee, Wisconsin, Spring 2009.

[46] Dr. J. Patrick (Pat) Donohoe, "Induction Machines II", class note for EECE 3414, Department of Electrical and Computer Engineering, Mississippi State University, Miss State, Mississippi.

[47] Ana Vladan Stankovic, Eric L. Benedict, Vinod John, Thomas A. Lipo, "A Novel Method for Measuring Induction Machine Magnetizing Inductance," *IEEE Transactions on Industry Applications,* Vol.39, No.5, pp 1257-1263, September/October 2003

[48] N.A.Demerdash, J.F.Bangura, "Characterization of Induction Motors in Adjustable Speed Drives Using A Time-Stepping Coupled Finite Element State Space Method Including Experimental Validation", Industry Application Conference, 1998.

[49] N.A.Demerdash, J.F.Bangura, A.A.Arkadan, "A Time-Stepping Finite Element-State Space Model for Induction Motor Drives Part 1: Model Formulation and Machine Parameter Computation", Electric Machines and Drives Conference, 1997.

[50] O.V.Thorsen, M.Dalva, "A Contribution to the Development of Transient models for Digital Simulation of Saturated Induction Machines with Deep Bar Effect", Electrotechnical Conference, 1994.

[51] V. Ostovic, *Dynamics of Saturated Electric Machines*. New York, Springer-Verlag, 1989.

[52] Bimal K. Bose, *Power Electronics and Variable Frequency Drives*. IEEE Press, 1996.